Science
AAAS

Supplementary Materials for

Methoxyl stable isotopic constraints on the origins and limits of coal-bed methane

M. K. Lloyd *et al.*

Corresponding author: M. K. Lloyd, mlloyd@psu.edu

Science **374**, 894 (2021)
DOI: 10.1126/science.abg0241

The PDF file includes:

Other Supplementary Material for this manuscript includes the following:

Materials and Methods

1. Sample descriptions and origins

We analyzed the methoxyl concentration and $\delta^{13}C$ value of coals and coal precursors that span a range of thermal maturities from pristine wood to high-volatile bituminous rank. The origin and geologic history of these materials are described briefly below. If not already powdered, materials were hand powdered and homogenized using a steel mortar and pestle prior to analysis.

Undegraded woods and lignin: Gram-sized quantities of powdered poplar, bamboo, and kraft lignin were obtained from the USC Stable Isotope Laboratory. Sample origins and descriptions are provided in ref. (*32*). The kraft lignin standard is used only for cross-calibration purposes and is not considered in the suite of natural materials shown in Fig. 1.

Belchatow lignites: Two low-grade brown coals (PL-4/384 and PL-11/384) were analyzed from the Belchatow coal district, Poland (*34*). The coals were deposited in a freshwater environment and rapidly buried in tectonic grabens 40 km long and ~1.5 km wide in the early Miocene (*34*). Reflectances of the vitrinite maceral ulminite present a narrow range of 0.26 to 0.29 $\%R_o$, categorizing these samples as low-maturity lignites.

Shimokita lignites/sub-bituminous coals: Six lignites and sub-bituminous coals were retrieved from 1.9–2.0 km below the sea floor ~50 km off the coast of the Shimokita peninsula, Japan (*13*, *35*, *36*). These 1–7 m thick coal horizons were deposited in a coastal, black marsh in the early/middle Miocene, and then buried to their current depth by slow subsidence in a forearc basin of the NE Japan Arc through the rest of the Cenozoic (*36*). These materials were retrieved from IODP site C0020 as part of IODP Expedition 337 (*35*). Conditions at the time of retrieval were reducing and alkaline: porewaters from the coal beds studied here had pH values of 7.5–9, alkalinity of 5–15 mM, and μM levels of dissolved H_2. The coals preserve authigenic carbonate and pyrite (*37*). In addition to observing active methanogenesis in these coal beds, 16S rRNA sequencing revealed taxonomic structures in these coal beds distinct from shallow marine communities and more resembling those found in modern coastal marshes, suggesting that the current microbial assemblages are indigenous descendants of the original microbial community entombed at the time of deposition, and that these assemblages have been degrading these coals in a closed system for the intervening ~20 Myr (*13*). Recent incubations of these coals on environmentally-representative substrates suggest that fermentative bacteria, not methanogenic archaea, dominate these assemblages, and are most active on other methyl-containing substrates such as trimethylamine and dimethylsulfide (*26*). Mean ulminite reflectances of these coals are 0.37 to 0.43 $\%R_o$, and broadly correlate with depth (*36*).

Powder River sub-bituminous coals: Two sub-bituminous coals from the Powder River Basin, WY were also analyzed. Although vitrinite reflectance data indicate that these coals are only marginally more thermally mature than the Shimokita coals (vitrinite reflectances of 0.45–0.47 $\%R_o$), they have experienced a more complex geologic history over a longer period of time (*38*). The Fort Union member sourcing these materials was

deposited in a freshwater, fluvial environment in the Paleocene, after which the unit was buried under erosional basin fill due to uplifts of the surrounding ranges associated with the Laramide Orogeny (*39*, *40*). The deepest sections of the unit reached at most 100 °C in the Miocene, after which continued uplift and erosion exposed the flanks of the basin to fresh infiltrations of nutrient-rich groundwaters, which continued until recent times (*39*). This marginal groundwater incursion may have been exacerbated by the natural combustion of exposed coal beds that enhanced permeability and the delivery of key nutrients (e.g., organic acids, SO_4^{2-}) to shallow subsurface coal beds along the flanks of the basin (*39*). This incursion stimulated a surge of secondary methanogenic activity along the basin rim, diluting 'old' methane, generated largely through hydrogenotrophic methanogenesis during the initial maturation phase, by the addition of 'new' methane, which bulk isotopic evidence suggests was produced by the methylotrophic pathway (*39*). This complex, spatially-varying history is also recorded in the scattered, contradictory biomarker biodegradation indices throughout the basin: characterization of soluble organic components in the Powder River Basin suggests that local geology and hydrology (i.e., permeability, recurring freshwater input) control the degree of biodegradation and methane production in any given site, not burial depth or vitrinite-based thermal maturity (*38*). Here, we consider samples from both endmembers: a sub-bituminous coal cored from the center of the basin where little secondary fluid is through to have reached (PR-FU-S352), and a less mature, more biodegraded sample from the northwestern basin margin with evidence for secondary microbial stimulation by shallow subsurface freshwater incursions (PR-FU-S939, *38*).

High-volatile bituminous coals from the Midwestern US: In addition to the above low-rank coals, we analyzed methoxyl contents from 6 more mature, high-volatile bituminous coals from the San Juan and Michigan basins (0.51–0.82 $\%R_o$). Although trace methoxyl groups were detected in some samples, these more mature coals did not contain sufficient methoxyl group abundance to determine their $\delta^{13}C$ values and we do not consider them further, other than to highlight that this observation is consistent with previous ^{13}C-NMR based studies of methoxyl loss during coalification, which suggest that virtually no methoxyl groups remain following the transition from sub-bituminous coal to high-volatile bituminous coal (*7*, *41*, *42*).

1.1 Artificial maturation experiments

Isotopic fractionations associated with the thermally activated reactions in kerogen and coal are often well-described by Rayleigh distillation (e.g., *16*, *43*). We performed a laboratory experiment to test whether this model holds for the specific case of thermally activated O-demethylation of wood. In order to directly observe a carbon isotope effect associated with O-demethylation of methoxyl groups, we artificially matured the poplar standard described above in two open-system, dry pyrolysis experiments. The experiments were designed to replicate the methods used in ref. (*44*), except for some key differences: 1) We pyrolyzed at a fixed temperature. This was done so that the isotope effect of O-demethylation could be measured and compared to model predictions from ref. (*17*), which are temperature-dependent, in a straightforward manner. We used a temperature of 300 °C because this was the lowest temperature at which significant O-demethylation would occur on a timescale where our experimental setup could be

maintained (hours to days). 2) We pyrolyzed wood in an open system, where evolved gases were continuously removed. This was done to target the reaction of interest: thermally activated O-demethylation by homolytic cleavage. The pyrolysis of plant matter creates various volatile species, notably methanol, chloromethane, acetaldehyde, and acetone, which have been shown to originate from ester-bound methoxyl groups in pectin (*25*, *45*, *46*). Wood contains some pectin, but since wood pectin is efficiently degraded during peat formation, peat and coals largely do not (*7*, *25*). Although the amount of secondary volatiles (chloromethane, methanol, etc.) released from wood is ~40× smaller than the amount of ether-bound lignin methoxyl groups, we were still concerned that secondary wood volatiles could back-react with remaining lignin methoxyl groups, which could add an additional O-demethylation mechanism that would not be present in coals, and alter the experiment. Therefore, we elected to continuously remove volatile products by freezing and vacuum evacuation over the course of the pyrolysis experiments.

Specifically, 298.1 or 416.0 mg of ground poplar were packed into a ¼'' Pyrex® tube that was flame-sealed on one end. The apparatus was evacuated on a vacuum line across Pyrex® U-trap immersed in an ethanol–CO_2 ice slush in order to trap moderately volatile reaction products (e.g., water, aromatics). Once evacuated, the tube was heated in a copper block at 300 °C for 12.5 or 34.0 hr. Volatile components were continuously removed by condensation and exposure to high-vacuum for the duration of the experiments. At the end of each experiment, the tube was opened, and solid material was recovered. The residual methoxyl contents and $\delta^{13}C$ values from these maturation experiments were determined by subjecting these chars to the same procedure described in Section 2.2, below (Table S4). The reflectance of these experimental products was not determined.

1.2 Study design rationale

This study uses the concentration and carbon isotopic composition of methoxyl groups in lignin and coals to constrain the mechanism by which coals are demethylated. This approach is inspired by an established precedent of using the carbon isotopic composition of methoxyl groups to distinguish degradation mechanisms in methyl tert-butyl ether (MTBE) and other environmental contaminants (e.g., *47*, *48*). In some cases, deuterium contents can add additional constraints (*47*). Such two-dimensional isotopic fingerprints can help distinguish reaction mechanisms that are indistinguishable with carbon isotopes alone. Although it would be possible to analyze methoxyl δD in our samples, such data would be unlikely to help address our research question for the following reasons:

1. The δD of methoxyl groups in undegraded wood are not uniform but rather depend on the δD of xylem water/precipitation in which the plant grew (*49*, *50*). Thus, modern wood methoxyl δD vary by >100‰ (*50*). Interpreting any change in methoxyl δD in our coals due to a degradation process would require correcting for this meteoric water signal. This is hard to do with confidence in materials >10 Ma old because other robust archives of xylem water δD (e.g., cellulose) no longer exist. In fact, wood methoxyl δD has shown promise as a proxy for paleo-precipitation in Eocene fossil wood precisely because other archives are scarce

(*51*). Even *if* it were possible to independently determine the δD of ancient source waters with high confidence, it would still not be possible to estimate initial methoxyl δD with an uncertainty of better than ± 20‰, which is the standard deviation of the mean isotopic fractionation between wood methoxyl groups and xylem water in modern trees (*50*). The methoxyl $\delta^{13}C$ approach employed in this study is useful because the isotopic signal of O-demethylation is >5× larger than the uncertainty on the initial isotopic composition (50‰ enrichment vs. a max initial range of 10‰). Considering that a methoxyl δD signal of O-demethylation would be a secondary isotope effect and initial values would have an uncertainty range of ~40‰, it is unlikely that methoxyl δD values would add a useful constraint to this study.

2. Interpretation of methoxyl δD values in these coals would require assuming that no processes other than O-demethylation alter δD during diagenesis. However, carbon-bound hydrogen atoms in organic compounds isotopically exchange with pore water on geologic timescales (e.g., *52*, *53*). Hydrogen isotopic re-equilibration is observed in organic molecules with thermal maturities as low as 0.4 $\%R_0$, which overlaps with the key samples studied here (*53*). Thus, we would be unable to rule out the possibility that hydrogen isotopic exchange had influenced the δD of the coal methoxyl groups studied here, further confounding interpretations.

2. Site-specific analytical methods

We used two different extraction and analysis procedures to measure and replicate the $\delta^{13}C$ values of methoxyl groups in coal and coal precursors. Both procedures employ the Zeisel method (*54*) to quantitatively derivatize methoxyl groups to iodomethane via the reaction:

$$R–O–CH_3 + HI_{(aq)} \rightarrow R–OH + CH_3I, \quad \text{(S1)}$$

Where R is any organic structure (e.g., aromatic ring, alkyl chain, etc.) that is ether- or ester-linked to the target methyl group. The first procedure is comparable to established methods for methoxyl extraction, online purification, and $\delta^{13}C$ measurement by compound-specific headspace gas chromatography (GC)-combustion-isotope ratio mass spectrometry (IRMS) (*55*), but modified to accommodate the analysis of materials with lower methoxyl contents by using larger vials, larger injection volumes, and longer reaction times. The second method is an off-line derivatization + sealed tube combustion + dual-inlet IRMS procedure previously described in (*56*), but modified to include additional purification steps. The first method generates accurate and precise methoxyl $\delta^{13}C$ values, but does not directly quantify the total methoxyl content of materials (c.f., *32*, *55*). The second method quantifies methoxyl content by manometry, but its methoxyl $\delta^{13}C$ values are potentially subject to the incorporation of organic contaminants in the sealed-tube combustion step.

Here we applied both methods to most samples. In addition to validating the main finding of this paper by obtaining comparable methoxyl $\delta^{13}C$ values by two independent techniques, this approach allows us to cross-calibrate our measurements in order to obtain more accurate estimates of methoxyl concentration. Below, we first describe each

procedure (Sections 2.1, 2.2), then describe the workflow for cross-calibrating these measurements (Section 2.3).

2.1 On-line GC-combustion-IRMS procedure

2.1.1 Methods

For each online extraction, 2–1200 mg of powdered material was loaded into a 12 ml borosilicate Labco Exetainer® vial with a heat-resistant screw-cap and gas-tight chlorobutyl septum. This was sealed and purged with ultra high purity helium (UHP He: 99.999 % purity, Airgas) for 5 minutes. Next, 0.5–4 mL of 57 % Hydriodic acid in H_2O (99.5 % purity, not stabilized, Sigma Aldrich) was added through the septa by injection with a gas-tight syringe. Sufficient acid was added to cover the powder for each experiment, so larger sample masses required more acid. The acid-sample mixture was sonicated, then immersed in a silicone oil bath held at 130 °C on a hot plate for 2 hours to convert methoxyl groups to iodomethane (CH_3I) (*55*). Samples were cooled and equilibrated at room temperature for at least 30 minutes prior to analysis.

On-line determinations of methoxyl $\delta^{13}C$ values were performed at Caltech using a Thermo GC-combustion-IRMS interface with the following procedure. For each analysis, 25–250 μL of vial headspace was extracted with a Hamilton Gastight® locking syringe and manually injected into a Finnigan TraceGC Ultra with an inlet chamber held at 120 °C in a He split flow of 10 mL/min (7:1 split ratio). To preclude memory effects, the syringe was cleaned after each injection by purging the needle and chamber 10× with UHP He. CH_3I was separated from other evolved compounds on a Phenomenex ZB-5ms column with an He carrier flow of 1.4 mL/min and a temperature program of: 30 °C for 15 minutes, then ramp at 20 °C/min to 120 °C. Eluted organic compounds were oxidized to CO_2 in a CuO-packed furnace held at 1000 °C, dried on a Nafion column, and analyzed for $\delta^{13}C$ and $\delta^{18}O$ at masses 44, 45, and 46 on a Delta V IRMS in continuous-flow mode. The iodomethane peak was identified based on retention time (~130s after injection), and observed to be fully resolved from other contaminant peaks (e.g., iodoethane, iodopropane, benzene, methylcyclopentane) in each run. Identities of iodomethane and other compounds were confirmed by analyzing an additional aliquot of the headspace of each sample on a separate GC-MS instrument outfitted with an identical column and subjected to the same temperature program.

2.1.2 Standardization of continuous-flow IRMS measurements

Four peaks of reference tank CO_2 were measured at the beginning and end of each GC run to account for mass spectrometric drift. To correct for inaccuracies associated with the combustion interface and calibrate $\delta^{13}C$ values onto the VPDB scale, a working lab standard containing eight fatty acid esters ("F8") was analyzed regularly (2–3× per week) during the three-week measurement session. The mean offset between measured and accepted $\delta^{13}C$ values for the fatty acid standards was invariant over the measurement session and independent of absolute $\delta^{13}C$ value over the calibration range (–23 to –31 ‰ vs. VPDB; mean standard offset = 0.71 ± 0.20 ‰, 1σ, n = 64). So, a single $\delta^{13}C$ offset correction of 0.71 ‰ was uniformly applied.

We verified the accuracy of the complete GC-combustion-IRMS procedure for iodomethane by regularly measuring headspace injections of a 400 mL gas-tight vessel containing a mixture of CO_2, methanol, iodomethane, and toluene standards. $\delta^{13}C$ values of the iodomethane standard were not correlated with peak size/injection size over the calibration range that brackets all reported samples ($r^2 = 0.002$), nor showed significant temporal drift over the course of the measurement session ($r^2 = 0.067$). The long-term mean of measured $\delta^{13}C$ values of the iodomethane standard was not significantly different from its external accepted value: measured $\delta^{13}C = –50.53 \pm 1.6$ ‰ vs. VPDB (1σ, n = 18) vs. external $\delta^{13}C = –52.3 \pm 0.1$ ‰ vs. VPDB; external value determined by sealed-tube combustion + dual-inlet IRMS (n = 5). So, no iodomethane-specific standard correction was applied on top of the F8-based standard.

A high-$\delta^{13}C$ CH_3I standard was not available for two-point calibration. However, the accurate measurement of the low-$\delta^{13}C$ CH_3I standard (at the ~2 ‰ level) suggests that any nonlinearity in the native $\delta^{13}C$ scale of the analytical system was minor relative to the range in CH_3I $\delta^{13}C$ values reported here. Moreover, as will be discussed below, the excellent agreement in CH_3I $\delta^{13}C$ values over a range of 50 ‰ (Fig. S1) from uncontaminated samples generated by separate extraction techniques (online vs. offline) and analyzed on two different mass spectrometers in different measurement modes (continuous flow vs. dual inlet) further supports that any scale compression effects are minor.

No CH_3I was detected in a full procedural blank where toluene (a methoxyl-free analogue for a lignin monomer) was reacted with HI acid, nor when an overmature, methoxyl-free anthracite coal was reacted. Therefore no blank correction was applied to the sample CH_3I data. In addition, no CH_3I was detected for a procedural replicate where a lignite coal was ‘reacted’ with deionized water instead of 57% HI acid; this test demonstrates that CH_3I was the product of the Zeisel reaction, specifically, and not merely a product of hydrous pyrolysis at 130 °C. This suggests that analyzed CH_3I products were derived from methoxyl groups, specifically, and not other methyl groups (e.g., *R*–C–CH_3) present in the samples. To improve precision, multiple headspace extractions from individual sample vials were performed, up to 5 times. Successfully resampling the same sample vial 10 days after initially piercing the septa demonstrated that 1) CH_3I is stable over day-to-week timescales while remaining in contact with residual HI acid and 2) any leakage of the vial that occurs during this time is minor and does not fractionate isotopes of carbon in CH_3I.

2.1.3 Discussion of poor reproducibility of the liquid CH_3I standard

Repeated headspace injections from the liquid CH_3I standard had significantly worse reproducibility (1σ of 1.6‰; n=18) than samples and solid standards (mean 1σ of 0.2‰; n=18). This disparity is likely due to CH_3I vapor pressure isotope effects, as has been recently discussed (Lee et al., 2019). The CH_3I standard vial had a condensed liquid phase, so isotopic scatter likely occurred when headspace aliquots were repeatedly extracted at an interval shorter than the timescale of vapor-liquid re-equilibration. In sample vials, CH_3I partial pressures were too low for a liquid CH_3I phase to condense. As

a result, sample data do not exhibit the same scatter, and CH_3I peak areas in these data were linear with methoxyl abundance (Figs. S2; S4; Lee et al., 2019).

Isotopic scatter and potential isotopic fractionation in the liquid CH_3I standard do not affect the accuracy or interpretation of our coal methoxyl data. Instrument stability and scale accuracy were monitored with regular injections of an "F8" fatty acid standard mixture, which were time-invariant and more precise (1 sigma of 0.2‰, n=64; see above). The liquid CH_3I standard was used only as a secondary monitoring standard, to verify the linearity of the VPDB scale down to ~–50‰, and rule out the existence of any CH_3I-specific analytical artifacts. The former concern ($\delta^{13}C$ scale linearity) was independently verified by the 1:1 agreement (at the <2‰ level) between coal methoxyl samples analyzed by two independent analytical methods over a range of >50‰ (Fig. S1). The latter concern (methoxyl $\delta^{13}C$ accuracy) was independently verified by the agreement between our isotopic analyses and external, published analyses of the same materials (Fig. S4). In no case were systematic isotopic offsets observed. It is possible that minor inaccuracies in our data exist at the sub-permil level. Carbon isotopic accuracy at this level would require analysis of external standards with a large isotopic range that are calibrated to the VPDB scale yet adhere to the principle of identical treatment of samples and standards. For methoxyl groups, such materials have recently been developed (Greule et al., 2019), but did not exist at the time of these measurements (2016–2017). Here we interpret 50‰ carbon isotopic enrichments in methoxyl groups and intrinsic scatter between similar samples at the level of 20‰. Because these isotopic signals are so large, and isotopic scatter is an inherent feature of the data (Sec. S2.4), neither systematic or random isotopic inaccuracies at the 2‰ level—if present—would affect the interpretation of our results.

2.2 Offline methoxyl extraction, purification, and analysis procedure

2.2.1 Methods

To convert methoxyl groups to CH_3I and isolate and analyze the reaction product using offline techniques, we used a gas-tight reflux + condensation reactor, glass vacuum line, and standard techniques for offline combustion and dual-inlet IRMS analysis. The method is described in ref. (*56*), and thus only summarized here. The reaction setup consisted of an N_2 inlet fed into a pear-shaped Pyrex reaction vessel that was connected in series to a coil-style, water-chilled glass reflux condenser, a glass triple-U trap, and a stainless steel 1/16" OD outlet capillary. For each extraction, 5 to 25 mL of cold (–4 °C) 57% aqueous HI acid (unstabilized, Sigma Aldrich) and 45 mg to 9.4 g of sample material were added to the reaction vessel, which was then sealed and purged with N_2 for 5 min at 80–100 mL/min. The N_2 rate was reduced to 30–80 mL/min, the glass triple U trap was immersed in an n-pentane + liquid N_2 slush (–131 °C), and the HI acid was heated to reflux (130 °C) using a hemispherical resistance heating mantle powered by a Variac® transformer at 70 V.

The reaction was run for 120 min, during which time methoxyl groups were derivatized to CH_3I via Reaction S1, carried through the condenser, and continuously frozen into the triple-U trap. Preliminary tests were unable to recover detectable quantities of CH_3I from coal residues that had already undergone this reaction, demonstrating quantitative conversion of methoxyl groups under these conditions.

Indeed, other studies report quantitative methoxyl derivatization at 120 °C in 30 min (*32*, *55*). Yield tests using known quantities of the monomers methanol, vanillin, syringin, and guiacol were also used to verify the yield of the reaction and subsequent purification. Yields in these monomer experiments were 90–105 % of theoretical yield based on stoichiometry.

Next, evolved CH_3I was purified from other volatile reaction products on a glass vacuum line using a series of cryogenic separations: First, residual N_2 was removed by gradually exposing the triple U-trap to high vacuum while immersed in liquid N_2 (30 min). Next, the gas mixture was distilled by warming the triple U-trap to room-temperature, and passing the gas across a vacuum trap immersed in an ethanol + CO_2 slush (–77 °C) and freezing it in another triple U-trap immersed in liquid N_2 (20 min). To remove CO_2, the mixture was frozen in liquid N_2, then thawed in an n-pentane + liquid N_2 slush to release CO_2 but leave CH_3I condensed, then the headspace was evacuated (5×15 min). Yields of CH_3I were calculated from the pressure of the gas in a vacuum trap of known volume at room temperature assuming ideal gas behavior. Pressure was measured via a Baratron capacitance manometer (MKS Instruments).

The carbon isotope composition of product CH_3I was determined by offline combustion + dual-inlet IRMS of the resulting CO_2. For each combustion, 10 to 100 μmoles of CH_3I were frozen with liquid N_2 from the vacuum line into in a pre-combusted quartz break-seal with 40–200 mg of copper(II) oxide (pre-combusted, CuO powder, 99.99 % pure, Sigma Aldrich) and 40 mg of silver foil (pre-combusted, soft silver capsule, CE Elantech), and flame sealed. Quartz tubes were combusted at 780 °C for 6–8 hr to convert the carbon in CH_3I to CO_2 by the reaction:

$$2CH_3I + 2Ag + 7CuO \rightarrow 2CO_2 + 2AgI + 3H_2O + 7Cu \quad \text{(S2)}$$

Product CO_2 was separated from H_2O using standard cryogenic procedures on a vacuum line, and sealed into a new Pyrex break-seal. $\delta^{13}C$ and $\delta^{18}O$ values of CO_2 were measured on a Thermo Delta V or MAT 253 IRMS in dual-inlet mode against a calibrated reference CO_2 tank (Oztech).

2.2.2 Verification of offline procedure

The accuracy of $\delta^{13}C$ values determined by this offline extraction, purification, combustion, and measurement procedure was verified by comparing results for an anhydrous methanol standard subjected to the full CH_3I derivatization + analysis procedure described in Section 2.1.2 with direct combustion of the underivatized compound by conventional sealed-tube combustion. The $\delta^{13}C$ values of three full replicate derivatizations of this methanol standard agreed within uncertainty with the $\delta^{13}C$ value of the methanol sample when measured by direct combustion + dual-inlet IRMS: mean CH_3I $\delta^{13}C$ = –25.32 ± 0.74 ‰ (1σ, n = 3) vs. –25.4 ± 0.1 ‰ (1σ, n = 3) (full procedure vs. direct combustion). Because all carbon in methanol is able to be derivatized by the Zeisel reaction (Eqn. S1), this test suggests that no significant isotopic fractionation is introduced by the procedure of CH_3I conversion and purification. It does

not however, test for the ability to resolve other contaminants produced during the reaction of HI acid with more complex materials.

2.3 Cross-calibration of methoxyl extractions and analysis methods

Both methods of methoxyl extraction and analysis allow determination of methoxyl concentration and $\delta^{13}C$ value, each with their advantages and disadvantages. The offline procedure directly determines methoxyl content by manometry, but $\delta^{13}C$ values from offline combustions are susceptible to contamination from other organic compounds that are inseparable from iodomethane by cryogenic techniques. Iodomethane from immature samples with abundant methoxyl groups such as wood and some lignites can reliably be isolated without contaminants in the offline method (*56*), whereas iodomethane from more mature and degraded coals can be harder to purify because of the increasing abundance of volatile contaminants and the larger sample masses required. Because the GC-combustion-IRMS procedure isolates iodomethane by chromatography, these methoxyl $\delta^{13}C$ values are potentially more robust. However, because this technique subsamples a portion of vial headspace, relating observed peak areas to absolute methoxyl abundance is less straightforward. As described below, we use the $\delta^{13}C$ values of samples where both methods agree to identify off-line measurements that are robust and contaminant-free.

Here, we use the results from both techniques in order to validate our $\delta^{13}C$ measurements and cross-calibrate measurements of methoxyl concentration. The workflow is as follows: *i*) we compare methoxyl $\delta^{13}C$ values determined by online and offline methods and identify the subset of samples that agree within ± 2 ‰; *ii*) we assume that offline determinations of $\delta^{13}C$ value that agree with the online $\delta^{13}C$ value indicate that the CH_3I in the offline method was successfully purified from other contaminants, and thus that the methoxyl concentration measured by manometry (in the offline method) is robust; *iii*) we use this subset of data to create a transfer function that relates relative CH_3I peak areas (from the online method) to methoxyl concentrations from the offline method; *iv*) we apply this transfer function to the remaining online data to compute methoxyl concentrations for samples where the offline extractions were not pure; *v*) we report online $\delta^{13}C$ values for all samples, and methoxyl concentrations derived either from offline measurements (for the subset with <2 ‰ agreement) or from the online CH_3I peak areas, using the calibration derived in *iv*).

We note that this approach assumes that all samples are homogeneous with respect to methoxyl concentration and carbon isotopic composition, such that different aliquots of the same material are directly comparable. This assumption is discussed in the next section (Section 2.4)

All twelve samples were analyzed using the online procedure and all but one using the offline one. For seven samples, online and offline $\delta^{13}C$ values agreed within 2 ‰ (Fig. S1). These seven were used to generate a relationship between normalized peak area (peak area/sample mass/injection volume) and methoxyl concentration (Fig. S2). Two methods of calibration were used: the entire data set was fit using a power law regression (Fig. S2a), and the high methoxyl abundance and low methoxyl abundance

samples were fit with separate linear regressions (Figs. S2b,c). That this calibration would follow a power law with an exponent <1 is consistent with a previous study that observed a nonlinear, muted relationship between CH_3I abundance and peak area for headspace GC injections (*32*). Both the power law regression and low-abundance linear regressions were forced through the origin. Slight differences in methoxyl concentration are observed for samples with low methoxyl abundances depending on whether the linear or power law calibration is used. However, because these data are interpreted in log space, and the calibrations are very similar, choice of calibration does not affect interpretations or conclusions. The figures and data discussed in the main text employ the power law relationship, but we reproduce Fig. 1 using the linear relationship, below (Fig. S9). These two figures are effectively indistinguishable.

All high methoxyl abundance materials had better than 2 ‰ agreements between offline and online $\delta^{13}C$ values, so measured offline methoxyl concentrations were used for all these data, and thus choice of calibration has no effect on these mean results (Fig. S2b). However, we use the uncertainties on both linear regressions to estimate the uncertainty on every reported methoxyl concentration. This approach assumes that the correlation among our entire calibration data set is the best estimate of the reproducibility of any single concentration measurement. It is agnostic as to the source of this scatter. Potential causes of scatter in methoxyl concentration measurements are considered in the next section.

2.4 Sample heterogeneity and other sources of scatter

The approach outlined in Section 2.3, above, presumes that samples are homogeneous in methoxyl concentration and isotope composition such that results from different sub-aliquots can be directly compared. Although wood sections are not uniform with respect to methoxyl concentration and isotope composition (e.g., wood lignin content varies over the course of the growing season, *57*, and methoxyl δ13C values are sensitive to climate on superannual timescales, *58*), wood slabs can be homogenized by milling and mechanical mixing (*56*). Homogenization of coals is less straightforward. All coals were ground to a coarse powder prior to analysis, but this may not be sufficient if significant heterogeneities exist at a scale smaller than the grain size.

Both contamination of offline extractions and intrinsic sample heterogeneity could contribute to the scatter observed in Figs. S1 and S2. Distinguishing between these sources of uncertainty is possible—to some extent—because the presence of organic contaminants in an offline extraction + sealed-tube combustion will perturb both the observed methoxyl concentration and $\delta^{13}C$ value in a predictable manner: assuming that the $\delta^{13}C$ values of the CH_3I and organic contaminant(s) endmembers differ by a fixed amount, deviations in $\delta^{13}C$ value and apparent methoxyl concentration due to increasing contamination will follow a trajectory that conforms to a simple binary mixing model (Fig. S3). Of the seven measurement pairs where significant differences in $\delta^{13}C$ between online and offline extractions are observed, three conform to the trajectory expected by this binary contamination model. Mismatches in methoxyl concentration and ^{13}C content for the other four measurement pairs cannot be explained by this framework, and are

instead suggested to result from fine-scale heterogeneity that is intrinsic to these materials.

3. Bulk analytical methods

3.1 TC/EA-IRMS analyses

Total oxygen and hydrogen contents, and total H isotope compositions of samples were determined by TC/EA-IRMS at the CU-Boulder Earth Systems Stable Isotope Laboratory of Prof. Katie Snell. Briefly, between 80 and 750 µg of material were weighed into 3.5 x 5 mm silver capsules and pyrolyzed at 1450 °C in the glassy carbon reactor of a Thermo Scientific TC/EA. Product H_2 and CO were entrained in an He stream at 90 ml/min and separated on a GC column packed with 5Å molecular sieve held at 85 °C. Sample gases were introduced in succession to a Thermo Scientific Delta V IRMS operating in continuous flow mode via open split in a Conflo IV. For each analysis, measurement of sample H_2 peak at masses 2 and 3 was preceded by two measurements of a reference H_2 tank, followed by a calibrated magnet jump to masses 28, 29, and 30 in order to observe the sample CO peak, then two peaks from a reference CO tank. The H_3^+ factor was determined 4–6 times at the beginning, midpoint, and end of each ~12-hour analytical session. The H_3^+ factor varied between 4.83 and 5.07 ppm/mV among all analytical sessions but remained stable to within 0.03 (1σ) within each session.

H and O contents were calibrated to H_2 and CO peak areas by pyrolyzing a benzoic acid standard ($C_7H_6O_2$) (100–1200 µg). The relationship between µg of O and CO peak area was strong ($r^2 = 1.0000$) and invariant during the 5 day stretch during which all analytical sessions were run, so a single calibration line was used for all measurements. No significant CO peak was observed above background during pyrolysis of empty silver capsules, so no blank correction was applied to the CO measurements of samples. Correlations between µg of H and H_2 peak area of benzoic acid standard were strong within each analytical session (r^2 of 1.0000, 1.0000 respectively), but significantly different from each other. So, separate H content calibrations were applied to each analytical session individually. The high intersession reproducibility and accuracy of determinations of the H content of a D-glucose standard ($C_6H_{12}O_6$, Sigma Aldrich, 99.9% purity)—7.01 ± 0.35 wt. % H, n = 6, 1σ among both sessions, vs. theoretical value of 6.71 wt. % H via molecular formula—supports this approach. No significant H_2 peak was observed above background during pyrolysis of empty silver capsules, so no blank correction was applied to H_2 measurements, either.

H isotopic compositions of samples were projected onto the VSMOW–SLAP scale by measuring international reference standards of known isotopic composition during each analytical session. Specifically, a linear calibration between raw δ^2H values vs. the reference tank and δ^2H values on the VSMOW–SLAP scale was generated by interspersing at least two replicate measurements each of three international reference standards of icosanoic acid methyl ester (Schimmelmann et al., 2016): USGS70 (accepted $\delta^2H_{VSMOW-SLAP} = -189.4 \pm 1.4$ ‰), USGS71 (accepted $\delta^2H_{VSMOW-SLAP} = -4.9 \pm 1.0$ ‰), and USGS72 (accepted $\delta^2H_{VSMOW-SLAP} = -189.4 \pm 1.4$ ‰). Raw δ^2H values of reference standards were indistinguishable between both analytical sessions, so a single scaling line was used for all measurements. No significant correlation between H_2 peak

area and δ^2H_{wg} of replicate standards was observed ($r^2 = 0.0832$), so no additional nonlinearity correction was applied. All reported samples have isotopic compositions within the calibration range of measured standards.

3.2 EA-IRMS analyses

Total carbon and nitrogen contents and isotopic compositions were determined by EA-IRMS in the CU-Boulder Earth Systems Stable Isotope Laboratory of Prof. Katie Snell. Briefly, between 0.1 and 1.5 mg of sample were weighed into 5 x 3.5 mm tin vials. These were combusted in the reactor cell of a Thermo Scientific Flash EA, under a 200 ml/min stream of O_2 in a column packed with chromium oxide (Cr_2O_3) and held at 1020 °C. Product CO_2 and NO_x compounds were entrained in an He carrier stream at 90 ml/min and passed through a Cu-packed reduction furnace held at 650 °C to reduce NO_x species to N_2. Product N_2 and CO_2 were separated on a packed GC column held at 60 °C. These analytes were introduced into a Thermo Scientific Delta V IRMS operating in continuous flow mode via a Thermo Scientific Conflo IV interface. Isotope ratios of N_2 and CO_2 were measured in succession on masses 28, 29, and 30 Da (for N_2) and 44, 45, and 46 Da (for CO_2). Two reference peaks were measured before (for N_2) or after (for CO_2) each sample peak.

Carbon and nitrogen contents were calibrated by comparing to known masses of an internal laboratory collagen standard with known C and N contents (47.6 and 17.4 wt. %, respectively). $\delta^{13}C$ values were corrected for nonlinearity and projected onto the VPDB scale using contemporaneous measurements of an acetanilide standard ($\delta^{13}C = -29.53 \pm 0.01$ ‰) and the collagen standard ($\delta^{13}C = -9.0 \pm 0.1$ ‰). $\delta^{15}N$ values were corrected for nonlinearity and reported relative to AIR using the same standards: acetanilide $\delta^{15}N = 1.18 \pm 0.02$ ‰; collagen $\delta^{15}N = 6.7 \pm 0.1$ ‰).

4. Description of normalization scheme for methoxyl concentrations

Tracking the progress of the O-demethylation reaction in coals requires normalizing the methoxyl concentration in every sample to the concentration initially present. Reconstructing the initial methoxyl concentration is not straightforward because the coalification process modifies other aspects of coal chemistry in conjunction with O-demethylation. During early diagenesis, microbes selectively consume major wood components such as cellulose, hemicellulose, and extractives—upwards of 60% of wood by mass—while leaving the lignin skeleton essentially intact (*7*). Throughout coalification, hydroxyl, carboxyl and other functional groups are lost, further modifying a sample's structure and chemical composition (e.g., see ref *59* for a review). As a result, trends in apparent methoxyl concentrations can be controlled by processes external to the specific reaction we study here. For example, 'raw' methoxyl concentrations (measured as wt.% methoxyl as a fraction of total mass) increase during the transition from wood to Belchatow lignite, as total mass loss outpaces the loss of lignin methoxyl groups, specifically (Table S1, *32*). Similar types of complications probably exist during the transition from lignite to higher-grade coals, though their effects are less obvious.

In order to track the progress of O-demethylation, specifically, in the absence of extraneous changes to sample chemistry during coalification, here we make the following normalizations:

i) For each sample, wt.% methoxyl concentration is first normalized to the total organic carbon content of the sample, and both numerator and denominator are normalized to their molecular mass. This step corrects for the dilution of methoxyl contents due to the inclusion of inorganic minerals in the sample. The resulting value represents the fraction of carbon atoms in the sample that are methoxyl carbons.

ii) Second, the methoxyl carbon fraction of each sample is normalized to the estimated lignin fraction; i.e., we divide each sample by the fraction of carbon atoms that are part of lignin or a lignin-derived structure. This step corrects for the dilution of methoxyl content due to the analysis of other organic components that do not contain methoxyl groups in their structure.

Together, this normalization scheme becomes:

$$\text{Methoxyl carbon fraction} = \frac{\text{wt.\% methoxyl}}{\text{wt.\% C}} \times \frac{\text{molar mass of C}}{\text{molar mass of } OCH_3} \times \frac{1}{\text{lignin fraction}} \quad \text{(S3)}$$

For the purposes of this scheme, we assign a lignin fraction of 0.25 for wood, and of 1.0 for all other samples. These values are consistent with typical compositions of woods (*60*), and the observation that lignin is the principal organic precursor for Type-III coals such as those measured here (*61*). Another assumption of this approach is that total carbon content is invariant. This is not strictly true because carbon content tends to increase during coalification due to the loss of other functional groups, as discussed above. In extreme cases, this would result in a scale expansion, as a virtual increase in total carbon content would make methoxyl groups appear more degraded than they actually are. However, over the relatively small range of maturities considered here, such an increase in carbon content is small and inconsistent (<10%, if at all; e.g., *62*). All samples but one have total carbon contents between 47 and 63 %. Because we interpret our data in log space, errors in true demethylation reaction progress in the range of ~20 % relative have little bearing on our data or their interpretation (Fig. S14). All wood methoxyl concentrations are converted to methoxyl carbon fraction (i.e., the fraction of all lignin-derived carbons that are methoxyl groups) assuming a wood lignin content of 25 % and a wood wt.% C of 45 % (*60*).

5. Calculation of methoxyl fraction of total methane generation potential

The carbon isotope composition of methane is commonly used to fingerprint its source, exploiting the fact that the fractionation factors of biogenic methane formation pathways are larger than the thermogenic ones (*15*, *30*). However, if the substrate for biogenic methane is anomalously enriched in ^{13}C (such as the coal methoxyl groups seen here), the methane produced could carry a $\delta^{13}C$ value that falls in the thermogenic domain. The importance of such 'cryptic' biogenic methane production depends on the

abundance of methane that could be produced by this mechanism as a fraction of the total methane likely to evolve from a coal. Here, we estimate this fraction.

In the Main Text, we show that O-demethylation in coals is a microbial process. The products of anaerobic O-demethylation are attractive substrates for methanogenesis. Therefore, it stands to reason that there exists a complete, microbial reaction pathway from coal methoxyl groups to methane that takes place in the deep subsurface. The details of this pathway are complex and hard to constrain. Here, we represent this process as the general case where coal methoxyl groups source microbial methane with the following simplified reaction series:

$$\text{Coal methoxyl group} \rightarrow \text{C1 intermediate} \rightarrow \text{methane}. \quad \text{(S4)}$$

The accuracy of this series depends on the exact identities of the C1 intermediate compound and the microbes responsible for each metabolic step, which are unconstrained. One plausible specific reaction series uses the methyl group in acetate (CH_3COOH) as the C1 intermediate:

$$R\text{–}O\text{–}{*}CH_3 + CO_2 + H_2 \rightarrow R\text{–}OH + {*}CH_3COOH, \quad \text{(S5)}$$

where *R* represents the rest of the coal structure. This is followed by:

$${*}CH_3COOH \rightarrow {*}CH_4 + CO_2. \quad \text{(S6)}$$

In both eqns. S5 and S6, the asterisk denotes the specific carbon atom derived from the coal methoxyl group (*63*, *64*). The first reaction (S5) is common to acetogenic bacteria that fix carbon via the Wood-Ljungdahl pathway (*65*). It is thought to be an important contributor to the acetate pool in anoxic, freshwater environments (*66*, *67*). The second reaction (S6) is the aceticlastic methanogenesis pathway, which is also believed to be the dominant source of methane in freshwater swamps, bogs, and sediments (*64* and references therein). We note that while this specific reaction series is plausible, other variants involving different C1 intermediates (methanol, formate) are also possible, and the following calculations are agnostic as to the exact identity of the C1 intermediate. Note that a simpler reaction series, where coal methoxyl groups are reduced to methane by a single methanogen, has also been observed (*12*). This case, too is consistent with the arguments presented below.

The enzymatic O-demethylation model presented in the Main Text predicts the carbon isotopic composition of methoxyl groups as a function of reaction progress (Fig. 1). Through mass balance, it also constrains the carbon isotopic composition of the O-demethylation reaction product (i.e., the C1 intermediate) at any one instant (Fig. 2). Because the carbon isotope systematics of methanogenesis are relatively well-constrained (*15*, *18*), in principle it should therefore be possible to predict the $\delta^{13}C$ value of the evolved microbial methane at any one time. However, the exact carbon isotopic composition of biogenic methane depends on many factors, including the metabolic pathway used (e.g., aceticlastic, methylotrophic, ± methoxydotrophic, *12*, *15*), the "openness" of the methane-generating reaction, and the isotopic composition of the methanogenic

substrate. In the reaction series presented above (eqn. S4), the $\delta^{13}C$ value of the methanogenic substrate pool (the C1 intermediate) will be dynamic, and evolve with time in a manner that depends at any one moment on the relative rates and isotopic fractionations of the first and second reactions (*68*). Therefore, the instantaneous methane $\delta^{13}C$ value will be similarly dynamic. While it may be possible to constrain these various factors in a lab setting over the course of the reaction, for reactions that occurred in the deep subsurface long ago, this is clearly not possible.

While predicting the dynamic microbial methane $\delta^{13}C$ value at any intermediate step of reaction progress is not feasible, estimating the 'final' $\delta^{13}C$ value of the cumulative methane evolved is. If reaction series S4 runs to completion, mass balance dictates that the abundance and ^{13}C content of the cumulative methane must equal the abundance and ^{13}C content of the coal methoxyl groups degraded. A key finding of this study is that the first reaction in S4 (O-demethylation) appears to go to completion. It is imaginable, then, that the methanogenic reaction (second rxn. In S4) will as well. Even if the methanogenic reaction is not quantitative (if, for instance, some significant fraction of the C1 intermediate is diverted to other fates, as per ref. (*31*)), it is likely that it will not be highly isotopically fractionating. The intrinsic carbon isotope effect of methanogenesis is only expressed if the reaction is incomplete and enzyme rate-limited (*18*). This is unlikely because intermediate metabolite pools in coal are small (*6*) and initial coal activation appears to be rate-limiting (*28*). Therefore, even with incomplete conversion of methoxyl groups to methane, the methane is likely to inherit a $\delta^{13}C$ value similar to the methoxyl pool at the onset of methanogenic conditions.

Not all lignin methoxyl groups are likely to end up contributing to a subsurface microbial coal-bed methane reservoir. It is clear from this study and previous work that some fraction of methoxyl groups are degraded during the peatification process. Methoxyl groups metabolized to methane before the establishment of a sedimentary cap layer will not accumulate in the subsurface, and instead escape to the atmosphere or are subsequently oxidized in overlying units. In the Main Text we therefore suggest that the methoxyl concentrations and ^{13}C contents of the Belchatow lignites are a reasonable representation of the methoxyl pool that is actually delivered to the deep subsurface. The Belchatow lignites have methoxyl concentrations of 6.6 to 9.6 wt.%, and $\delta^{13}C$ values of –19 to –13 ‰ (Table S1). If these methoxyl groups are quantitatively converted to methane, they would yield up to:

$$\frac{9.6\ \text{g OCH}_3}{100\ \text{g coal}} \times \frac{1\ \text{mol OCH}_3}{(16.0+12.0+3\times1.0)\ \text{g OCH}_3} \times \frac{1\ \text{mol CH}_4}{1\ \text{mol OCH}_3} \times \frac{1000\ \text{mmol}}{1\ \text{mol}} = 3.1\ \text{mmol/g}$$ of methane.

This microbial methane would have a $\delta^{13}C$ value close to –19 to –13 ‰. Methane with a $\delta^{13}C$ value greater than –50 ‰ vs. VPDB is canonically considered thermogenic (*15*, *30*). Therefore, this 2–3 mmol/g of methane could be considered "cryptic" biogenic methane.

The total biogenic methane yield of a coal is hard to predict, and will depend on a variety of factors, as described in the Main Text. The cumulative thermogenic methane yield from coals is somewhat more regular, and provides a useful comparison point for understanding the size of this cryptic microbial methane pool. Specifically, the

thermogenic methane yield of a humic (type-III) coal is typically quoted at 6 Mcf (=10^3 standard cubic feet) per short ton (*69*, and references therein), which in SI units corresponds to:

$$\frac{6000\ \text{std cubic feet}}{\text{short ton}} \times \frac{1\ \text{short ton}}{907.18\ \text{kg}} \times \frac{1\ \text{kg}}{1000\ \text{g}} \times \left(\frac{0.3048\ \text{m}}{1\ \text{ft}}\right)^3 \times \frac{1\ \text{atm}}{288.7\ \text{K}} \times \frac{101325\ \text{Pa}}{1\ \text{atm}} \times \frac{\text{K·mol}}{8.314\ \text{m}^3\text{·Pa}} = 7.9\ \text{mmol/g}$$

.

Thus, cryptic biogenic methane from methoxyl groups can comprise ~40 % of the total thermogenic methane yield. This calculation suggests that it is a significant methane flux, and contributions of this anomalously ^{13}C enriched methoxyl methane to the total biogenic methane pool would measurably raise the cumulative $\delta^{13}C$ value of microbial coal-bed methane.

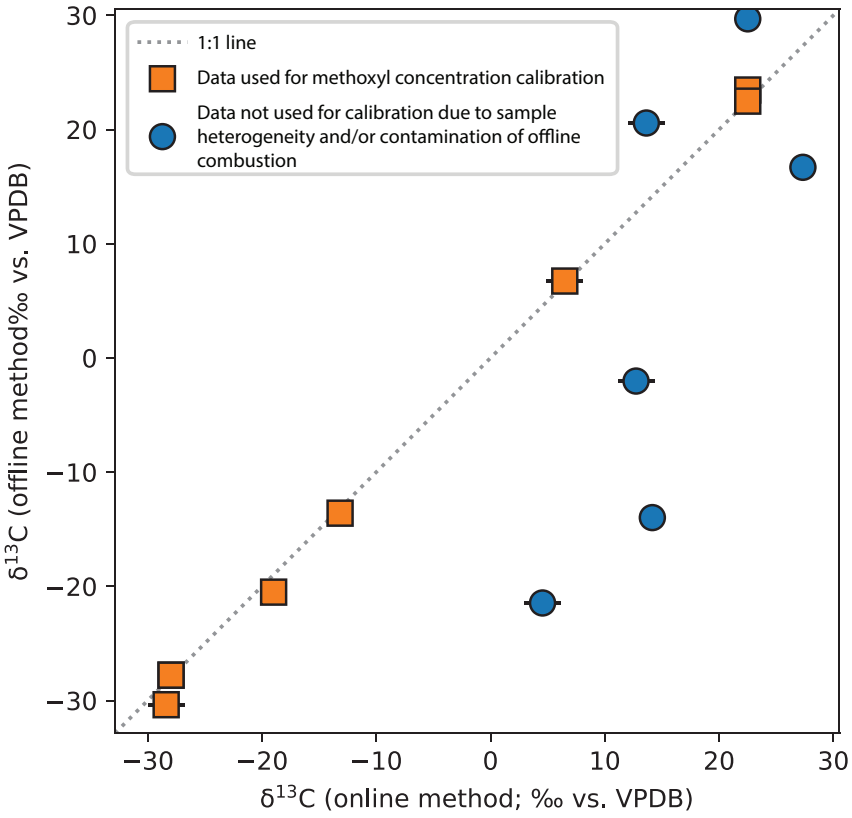

Fig. S1.

Comparison of methoxyl $\delta^{13}C$ values determined using the offline (sealed-tube combustion) procedure vs. the online (GC-combustion-IRMS) procedure. Each symbol represents an individual offline extraction + sealed-tube combustion, plotted against the mean $\delta^{13}C$ value of the same material measured online. Orange squares indicate samples where offline and online $\delta^{13}C$ values agree within 2 ‰. Based on this agreement, this subset is used to produce the concentration calibration shown in Fig. S2. Blue circles indicate other data with worse agreement between methods, most likely due to the inclusion of other volatile organics in the samples combusted offline. However, some degree of inhomogeneity in these materials may also cause this scatter (see Materials and Methods section 2.4 for details). 1:1 line also shown for comparison.

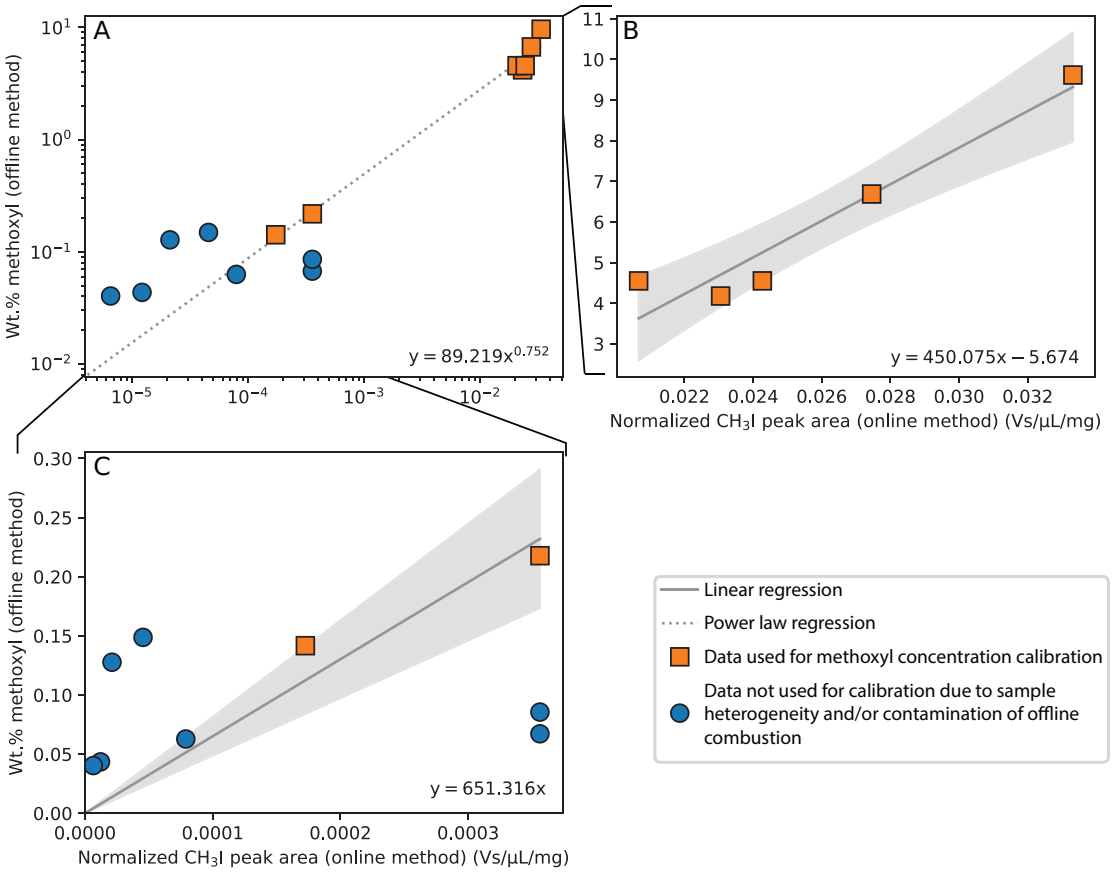

Fig. S2

Methoxyl concentration calibrations relating CH_3I peak area (measured using online GC method) to methoxyl concentration (measured by manometry using offline extraction method). Peak areas are normalized to the injection volume and sample mass. Only samples where online and offline methoxyl $\delta^{13}C$ values agree within 2 ‰ are used for calibration fit (orange squares), but all other samples are additionally shown for comparison (blue circles). Only the first, largest, online injection from each vial is used, as subsequent injections deplete the headspace CH_3I. Semi-transparent square showed acceptable agreement between methods w.r.t $\delta^{13}C$ value, but evidently poor agreement w.r.t methoxyl concentration, and is omitted from the calibrations (a and c; See Materials and Methods section 2.4 for details). Two types of calibration fits are shown. a): power law fit to the complete dataset. Note that this fit is performed on the dataset using linear axes, but shown here with logarithmic axes for clarity. b) and c): linear fits to subsets of the data, separating the (b) high-methoxyl materials and (c) low-methoxyl samples. The linear regression of low-methoxyl samples in c) is forced through the origin. The linear regression of high-methoxyl samples in b) is not. Shaded areas indicate 95% confidence intervals on linear regressions. We prefer the power law fit (a) because it is a continuous function, but provide an alternative version of Fig. 1 from the main text that uses the discrete linear regressions (b, c) as well (Fig. S9). Results are not sensitive to the choice of methoxyl concentration calibrations.

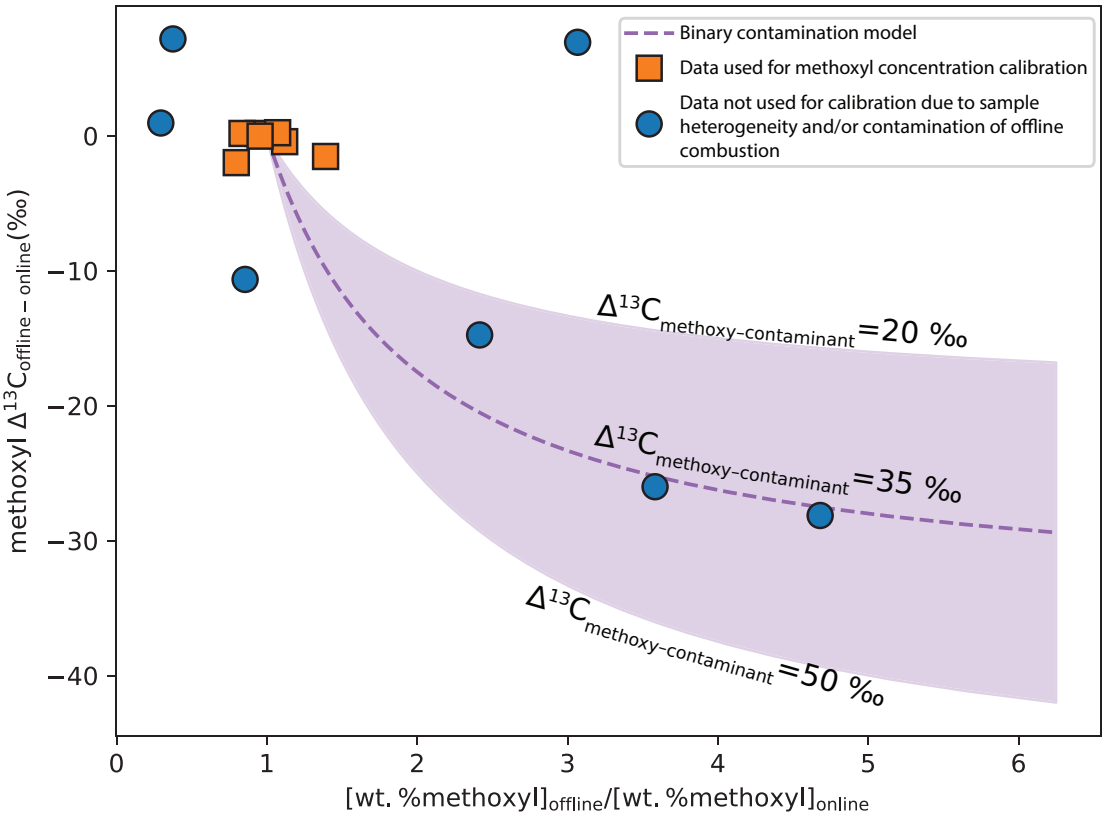

Fig. S3

Coupled effect of contamination on methoxyl concentration and $\delta^{13}C$ values from offline method. Binary contamination model assumes linear mixing between an endmember CH_3I component and an organic contaminant that differ in $\delta^{13}C$ value by 20–50 ‰. More complex contamination vectors are possible if S and N-bearing contaminants are considered, which would evolve a variety of S-bearing and NO_x species during sealed tube combustion that could generate isobaric interferences with the principal ion beams of CO_2 during the dual-inlet IRMS measurement. Sample homogeneity is another factor contributing to noise on this plot.

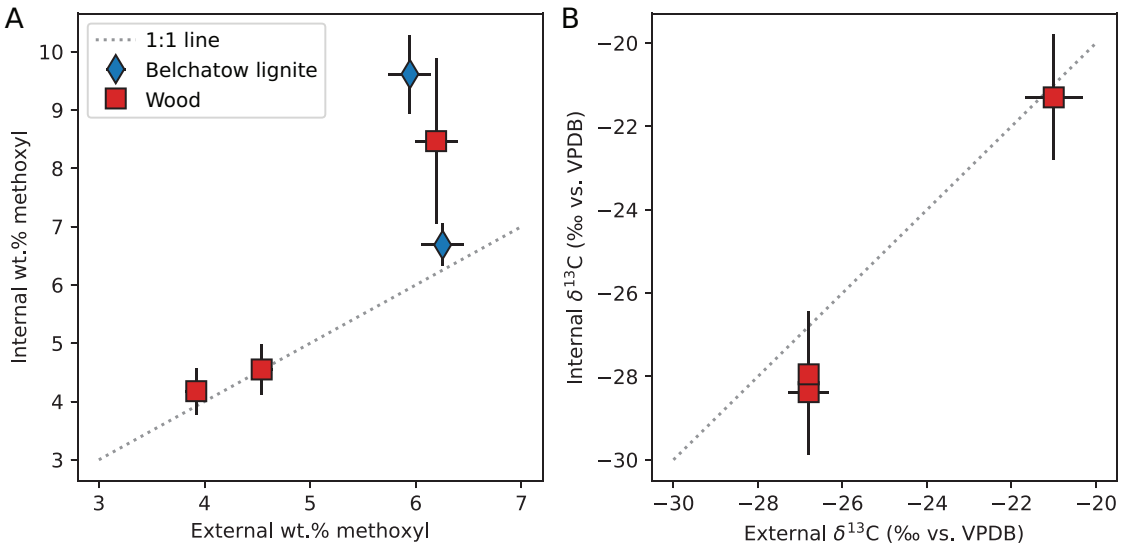

Fig. S4

Accuracy tests of methoxyl concentration and $\delta^{13}C$ value. a) our measured methoxyl concentrations ("internal") are compared to external values from ref. (*32*), generated using a different technique on sub-aliquots of the same starting materials. b) our measured methoxyl $\delta^{13}C$ values ("internal") compared to published values ("external", *32*) obtained on sub-aliquots of the same materials. 1:1 lines shown in both panels for comparison.

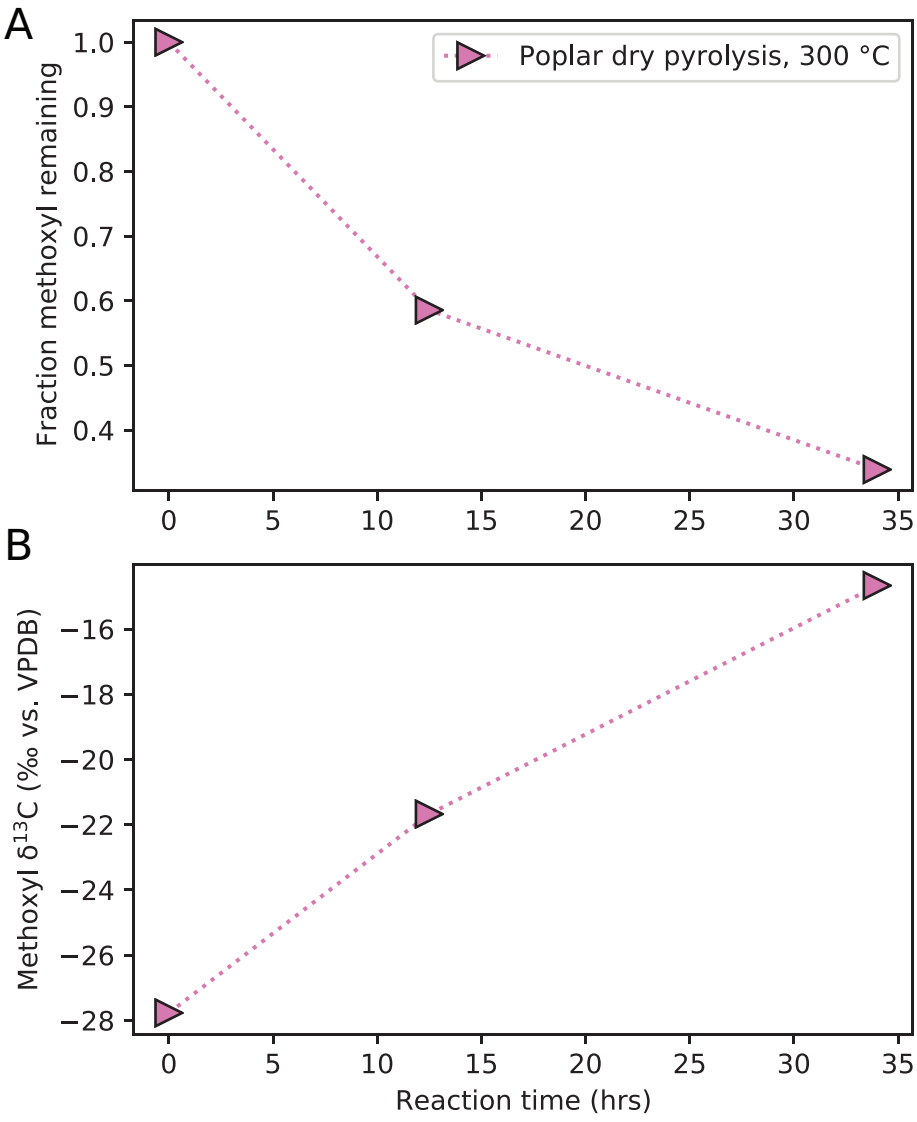

Fig. S5

Results of dry, open-system pyrolysis of poplar wood. A) Fraction of methoxyl groups remaining during pyrolysis. B) $\delta^{13}C$ values of residual methoxyl groups in reaction product.

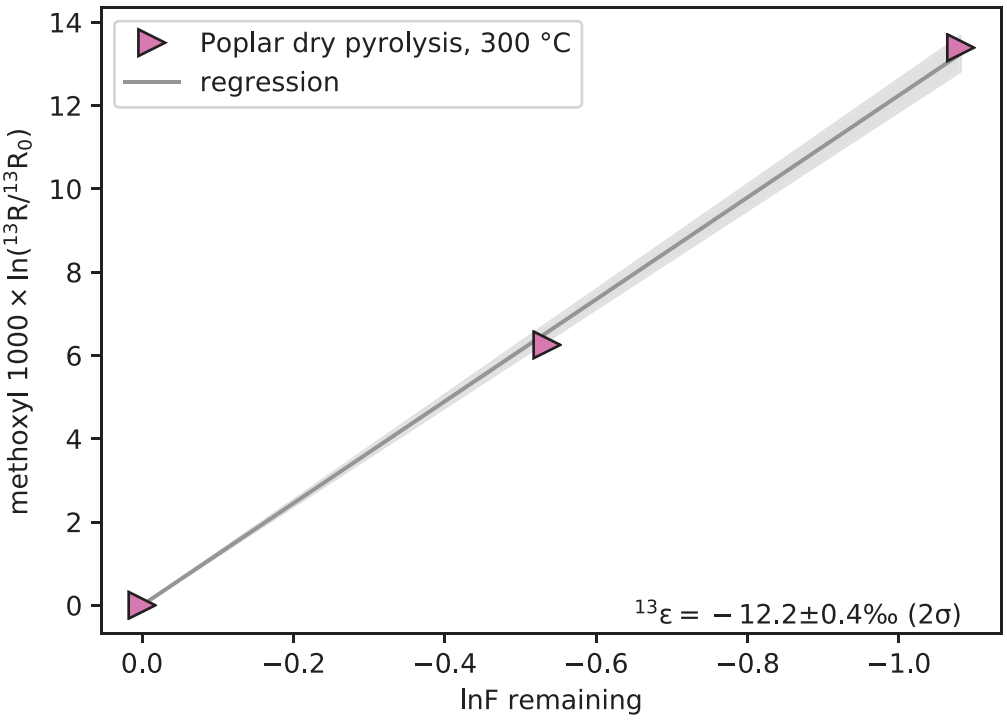

Fig. S6

Demethylation reaction progress and methoxyl carbon isotopic composition of dry, open-system poplar pyrolysis experiments. Data are fit by a Rayleigh fractionation model, which equates to a linear regression (dark grey line) with a y-intercept of zero for the axes shown. Slope of regression provides the instantaneous fractionation factor: $^{13}\varepsilon = -12.2 \pm 0.4$ ‰ (2σ). Light grey shading indicates 95% confidence interval on regression.

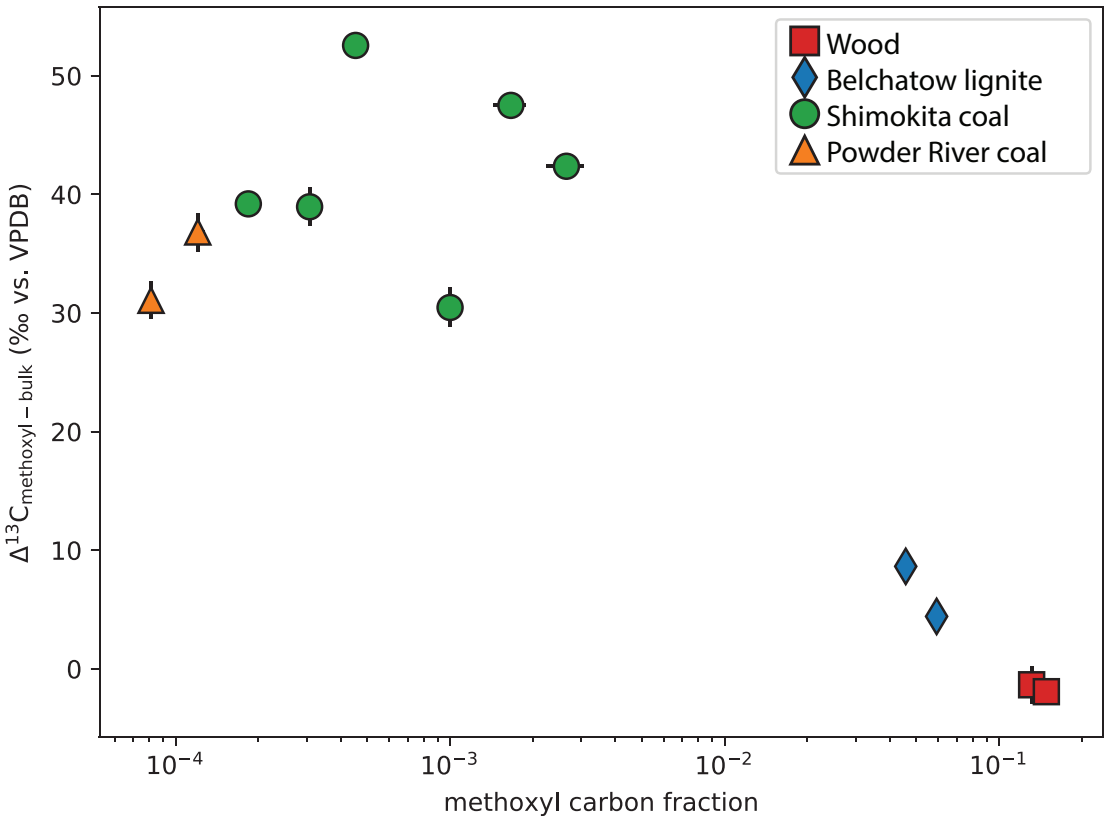

Fig. S7

Changes in methoxyl $\Delta^{13}C$ value ($\delta^{13}C_{methoxy} - \delta^{13}C_{bulk}$) vs. methoxyl carbon fraction (decimal fraction of all organic carbon atoms in a sample that are methoxyl groups). Wood methoxyl carbon contents are corrected for dilution by non-methoxyl bearing compounds (e.g., cellulose, hemicellulose) assuming a wood lignin fraction of 0.25.

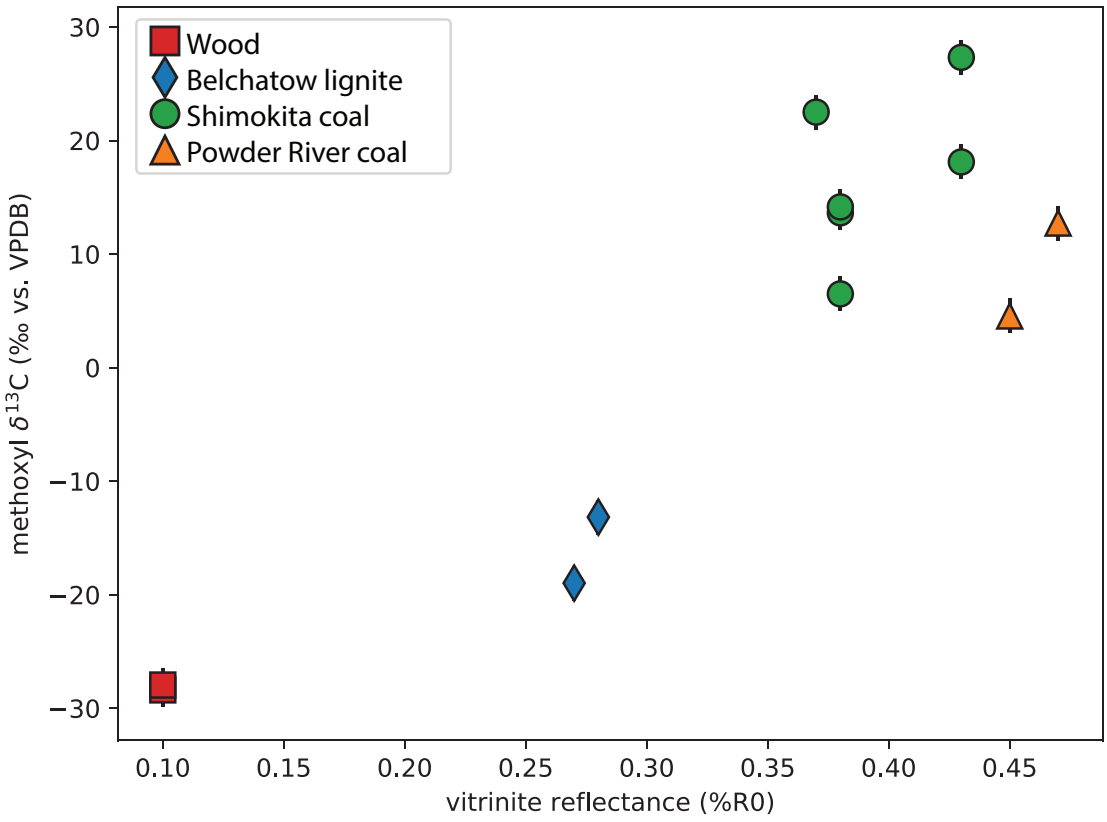

Fig. S8

Methoxyl $\delta^{13}C$ value vs. vitrinite reflectance, a proxy for thermal maturity. Vitrinite reflectance of pristine woods (red squares) were not measured, and are assigned a value of 0.1 for plotting purposes. Although a strong correlation between methoxyl $\delta^{13}C$ value and vitrinite reflectance is observed among all materials, within the lignite and sub-bituminous coals, no significant correlation is apparent.

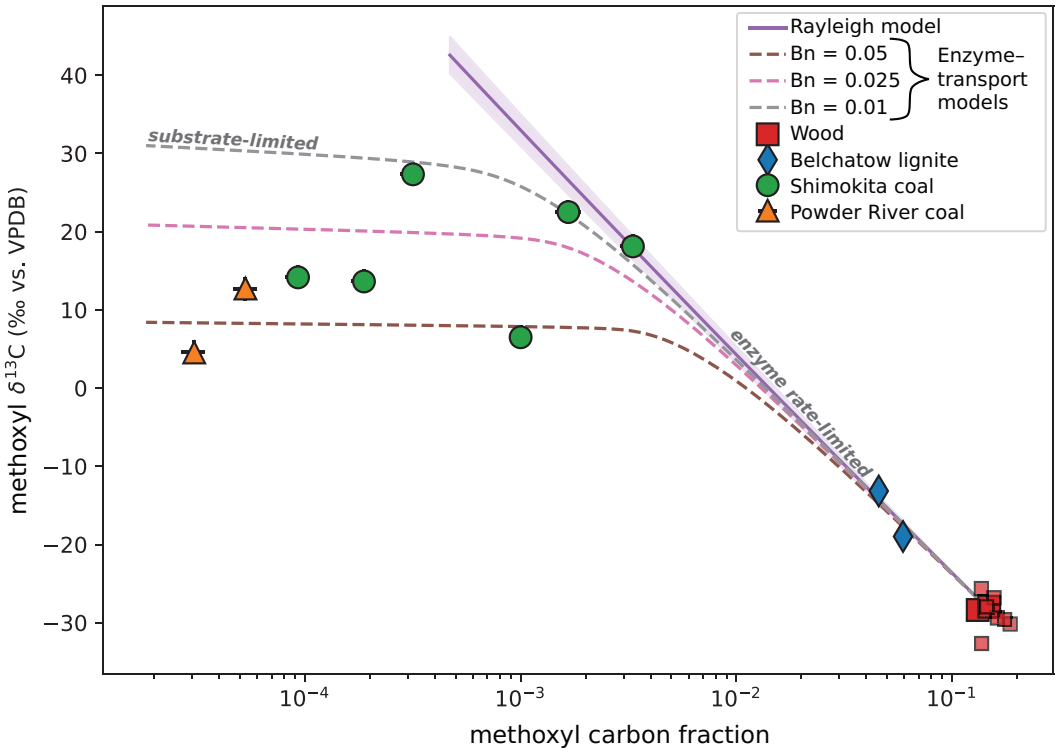

Fig. S9

Reproduction of key components of Fig. 1b in the main text, using an alternative concentration calibration scheme (discrete, linear regressions, Figs. S2b,c). The two different calibration schemes generate data that are effectively indistinguishable on a log scale. Choice of calibration scheme does not affect our results or conclusions.

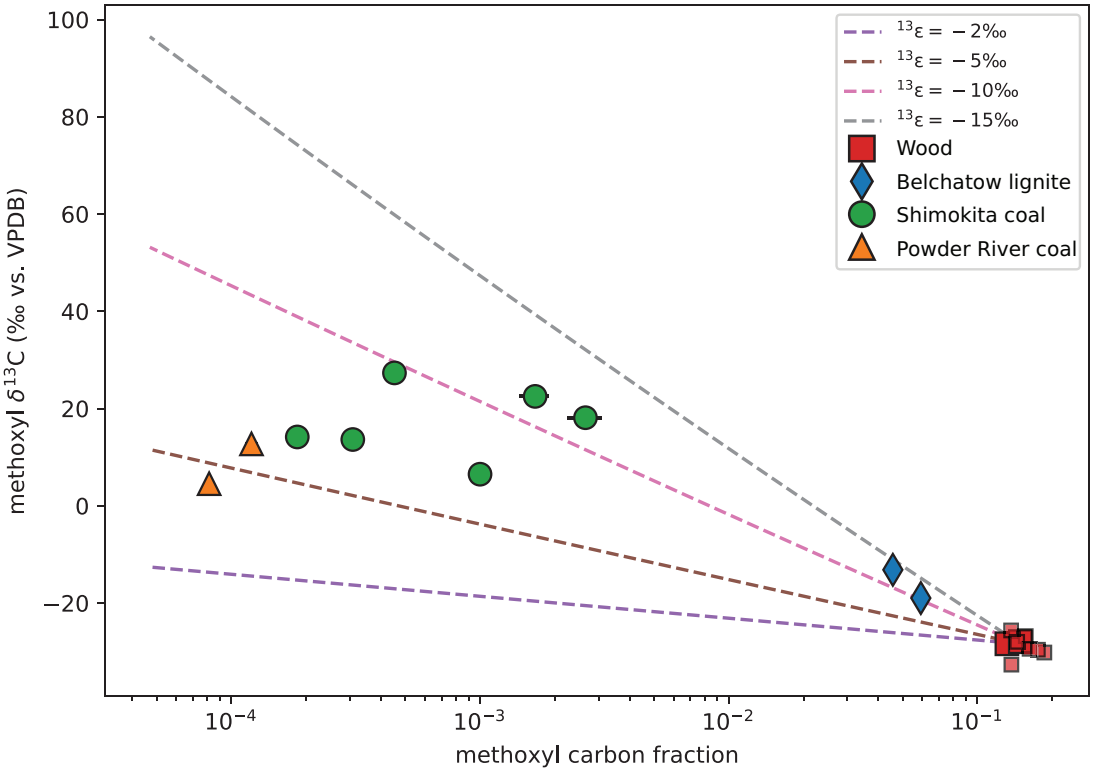

Fig. S10

Methoxyl data compared to Rayleigh fractionation models for a range of isotope fractionations for demethylation. Each datum could be described by an individual Rayleigh fractionation model between with an isotope effect between –2 and –12 ‰. However, we can think of no reason why the isotope effect should vary so strongly between similar (and often closely related) samples. Therefore, we consider this family of models an unlikely explanation for these data.

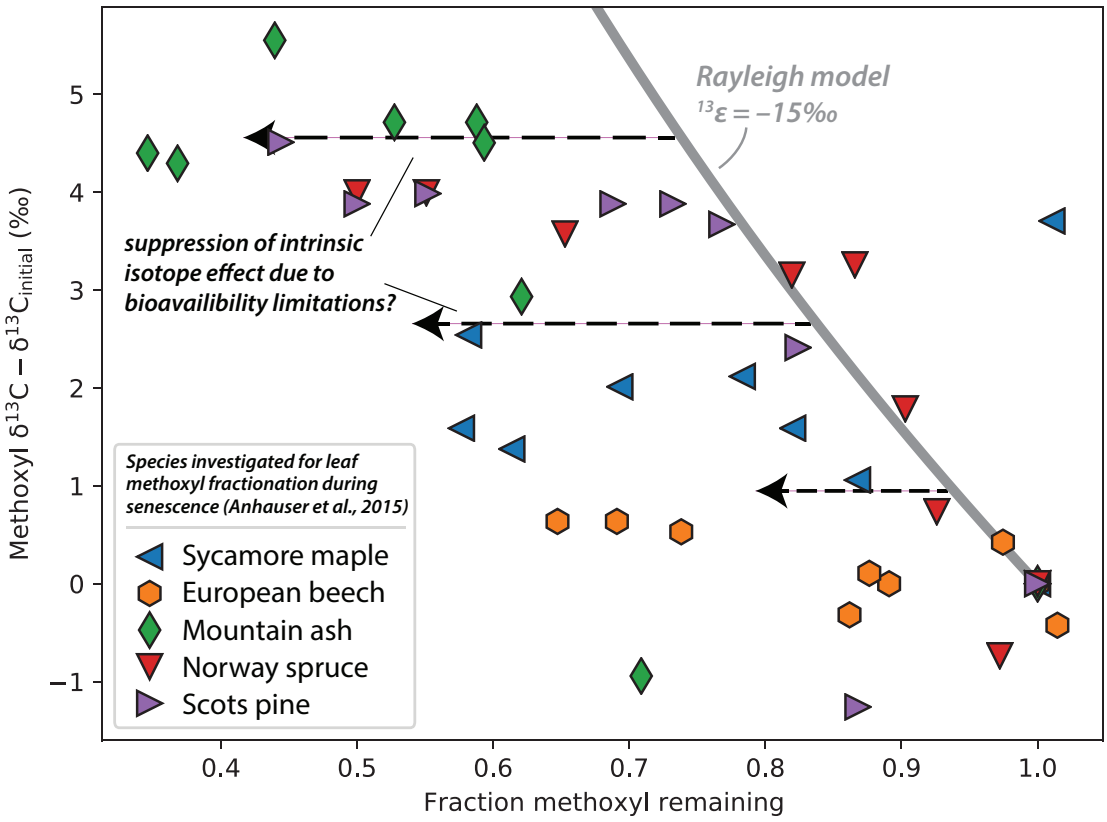

Fig. S11

Isotopic fractionation of methoxyl groups in leaves during multi-year leaf litter senescence experiments (*78*). To plot all data on the same scale, each methoxyl concentration and $\delta^{13}C$ value are normalized to the initial, undegraded value for that species collection, such that the initial composition for each series lies at the origin. Methoxyl degradation processes in leaves are potentially more complex than in coals because multiple compounds in leaf tissue with different preservation potential contain significant amounts of methoxyl groups (lignin, pectin), often with different ^{13}C contents (*88*). In fact, in the original study that obtained the data shown in this figure, increases in leaf methoxyl $\delta^{13}C$ were principally attributed to the preferential degradation of pectin methoxyl groups (*78*). An additional factor contributing to the scatter in these data could be enzyme-catalyzed O-demethylation reactions operating under variable degrees of mass transport limitations, analogous to the enzymatic model presented in the Main Text for humic coals, but operating at a different scale. In such a case, the largest isotopic fractionation observed in these data ($^{13}\varepsilon \approx -15$ ‰) is a lower limit on the intrinsic fractionation factor for enzymatic O-demethylation.

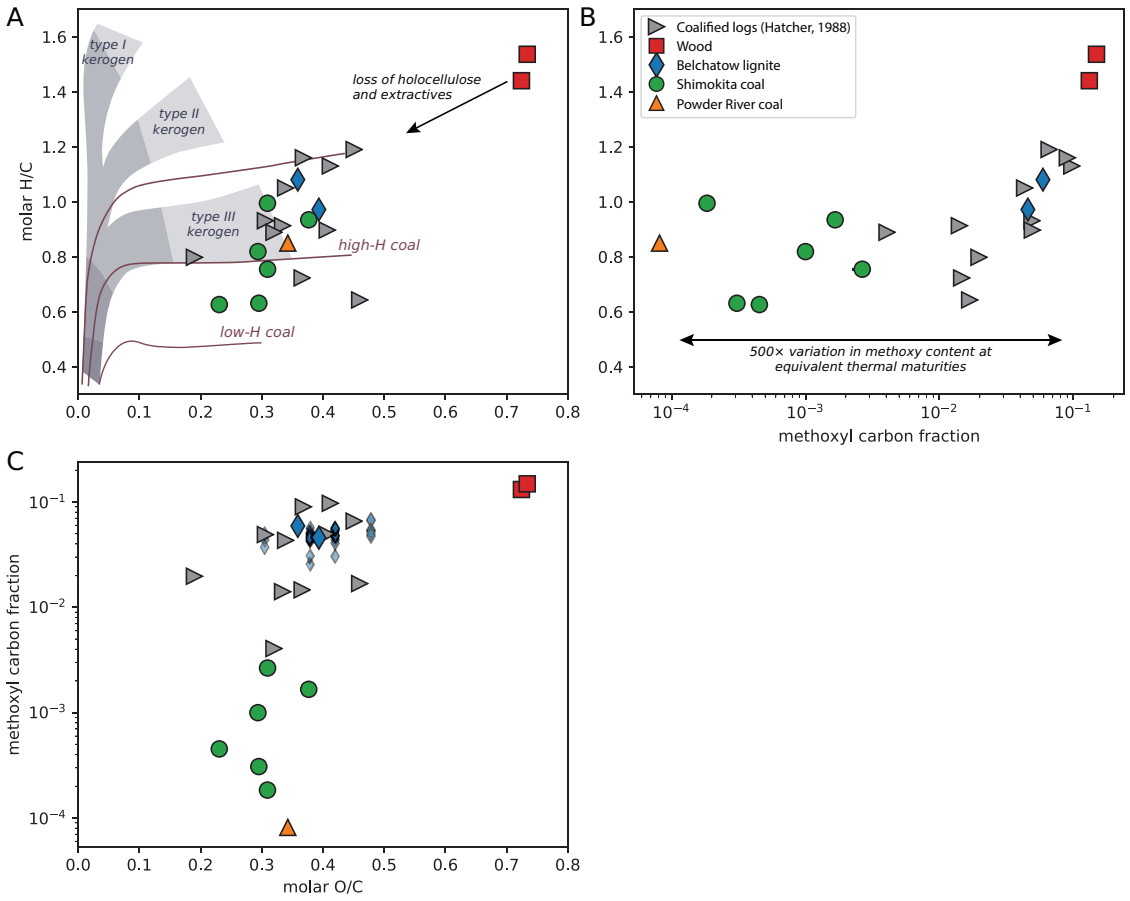

Fig. S12

Plots of molar H/C, molar O/C, and methoxyl carbon fractions of wood, coalified wood, and coal. A) van Krevelen diagram of wood and coals from this study, along with coalified logs from refs. (*41*, *62*). Fields for typical kerogen and coal trends from ref. (*61*). B) Molar H/C vs. methoxyl carbon fraction. C) Methoxyl carbon fraction vs. molar O/C. Methoxyl carbon fractions span 3 orders of magnitude at equivalent O/C and H/C ratios. Systematic differences in methoxyl concentration are observed between intact coalified logs and macerated matrix coals at the same levels of maturity. Methoxy carbon fractions from coalified logs obtained by multiplying reported percent methoxy/aromatic value by the aromatic carbon fraction for each sample.

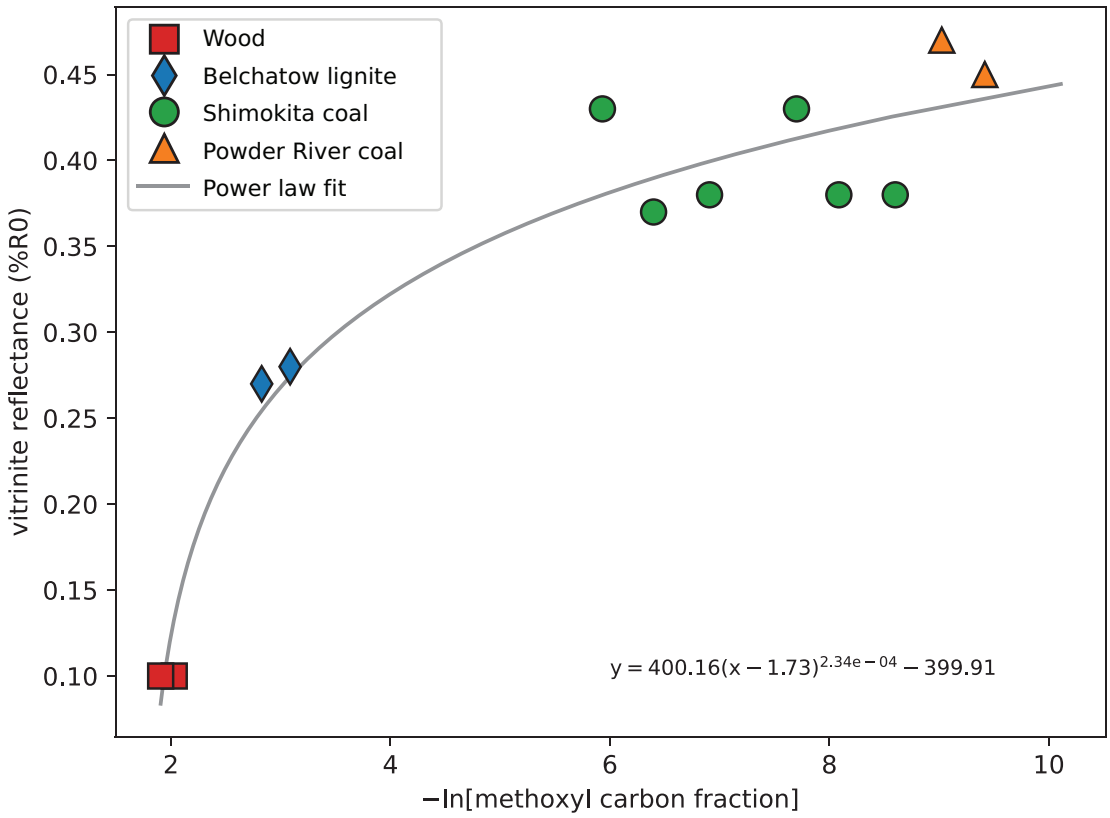

Fig. S13

Relationship between vitrinite reflectance and the natural log of methoxyl carbon fraction. Grey line is the power law fit to these data (equation shown on plot). This equation is used to convert methoxyl carbon fractions from the enzyme-transport model for O-demethylation to predicted vitrinite reflectance in order to depict the model on Fig. 2 in the main text.

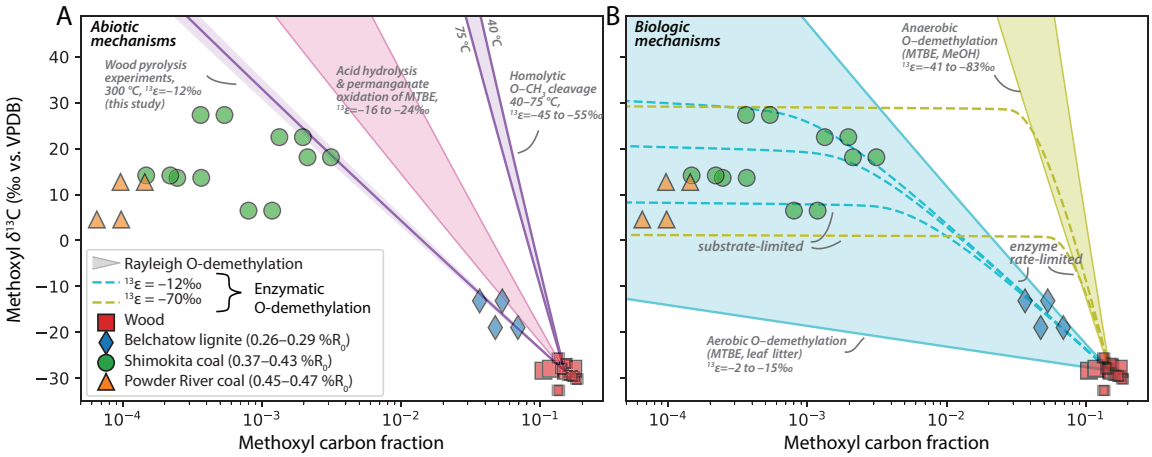

Fig. S14

Reproduction of Fig. 1 from the Main Text showing each datum with an error in methoxyl carbon fraction of ± 20% relative. This error range is a conservative estimate of the accuracy of our computations of the progress of the O-demethylation reaction (See Section S4 for details). The similarity of these data sets suggests that our conclusions are robust with respect to the exact estimate of reaction progress in any one sample.

Table S1.

Summary table of methoxyl concentrations, $\delta^{13}C$ values, and whole-sample C, H, and O contents and isotope compositions. All data shown here used for Figs. 1 and 2 in the Main Text.

Type	Name	Age	%R_o [+]	N[†]	Wt.% methoxyl[‡]	±1s.e.[ˇ]	Methoxyl $\delta^{13}C$ (‰ vs. VPDB)	±1s.e.[ˆ]	Wt.% C[“]	±1σ	Bulk $\delta^{13}C$ (‰ vs. VPDB)	±1σ	Wt.% H[“]	±1σ	Bulk $\delta^{2}H$ (‰ vs. VSMOW)	±1σ	Wt.% O[“]	±1σ	Molar O/C	Molar H/C	Methoxyl carbon fraction[*]	±1s.e.
Wood	USC Bamboo	Modern		1	**4.177**	0.396	-28.4	1.6	54.0	2.0	-27.0	0.1	6.0	0.2			47.5	0.7	0.66	1.31	1.20E-01	1.14E-02
Wood	USC Poplar	Modern		4	**4.550**	0.436	-27.9	0.1	53.0	1.0	-26.0	0.1	6.1	0.2			46.3	0.8	0.66	1.37	1.33E-01	1.27E-02
Belchatow lignite	PL-4/384	early Miocene	0.27	2	**9.616**	0.674	-19.0	0.1	62.9	1.6	-23.4	0.2	5.7	0.3	-111.6	8.8	30.1	0.4	0.36	1.08	5.92E-02	4.15E-03
Belchatow lignite	PL-11/384	early Miocene	0.28	2	**6.688**	0.362	-13.2	0.1	56.7	4.9	-21.8	0.1	4.6	0.2	-108.7	1.4	29.7	0.3	0.39	0.97	4.57E-02	2.47E-03
Shimokita coal	IODP-337 15R3	early/mid Miocene	0.38	1	0.048	0.004	13.6	1.6	61.0	1.3	-25.3	0.1	3.2	0.3	-131.9	0.8	24.0	0.7	0.30	0.63	3.08E-04	2.37E-05
Shimokita coal	IODP-337 15R4	early/mid Miocene	0.38	1	**0.142**	0.014	6.5	1.6	54.9	0.2	-24.0	0.5	3.8	0.1	-125.4	11.3	21.5	1.3	0.29	0.82	1.00E-03	1.00E-04
Shimokita coal	IODP-337 15R7	early/mid Miocene	0.38	2	0.027	0.002	14.2	0.3	57.4	0.6	-25.0	0.1	4.8	0.7	-133.3	5.1	23.7	1.4	0.31	0.99	1.84E-04	1.17E-05
Shimokita coal	IODP-337 18R2	early/mid Miocene	0.37	3	**0.218**	0.029	22.5	0.2	50.6	6.5	-25.0	0.9	4.0	0.2	-126.6	2.1	25.4	0.6	0.38	0.93	1.66E-03	2.24E-04
Shimokita coal	IODP-337 22R5	early/mid Miocene	0.43	3	0.073	0.006	27.3	0.3	62.8	2.7	-25.2	0.3	3.3	0.2	-127.3	0.4	19.3	1.5	0.60	0.63	3.17E-04	4.01E-05
Shimokita coal	IODP-337 25R	early/mid Miocene	0.43	2	0.424	0.067	18.1	0.1	61.9	1.3	-24.3	0.1	3.9	0.1	-110.6	3.5	25.5	0.5	0.31	0.75	2.65E-03	4.19E-04
Powder River coal	PR-FU S352	Paleocene	0.47	1	0.018	0.001	12.7	1.6	57.8	1.0	-24.1	0.3									1.20E-04	6.70E-06
Powder River coal	PR-FU S939	Paleocene	0.45	1	0.011	0.001	4.6	1.6	53.6	3.2	-26.5	0.1	3.8	0.2	-141.1	1.7	24.5	0.1	0.34	0.85	8.14E-05	3.88E-06
Indiana coal	USB 2-22-50	Pennsylvanian	0.51	1	n.d.																	
Springfield coal	Patiki mine	Pennsylvanian	0.55	2	n.d.																	
Springfield coal	Bear Run mine	Pennsylvanian	0.75	1	n.d.																	
Fruitland coal	SJB D395	Late Cretaceous	0.55	1	n.d.																	
Fruitland coal	SJB S057	Late Cretaceous	0.82	1	n.d.																	

[†]number of replicate injections from the same reaction vial used to determine methoxyl $\delta^{13}C$ value by the online GC-combustion-IRMS method. Only the first injection from each vial is used for the methoxyl concentration calculation (see [‡], below), but all injections are used to determine the average $\delta^{13}C$ value for each sample.

[‡]methoxyl concentration, derived from calibrations shown in Fig. S2. Bold numbers indicate samples that anchor the concentration calibrations (orange squares in Fig. S2), based on the agreement between $\delta^{13}C$ values from offline and online determinations (Fig. S1). For these samples, offline concentrations are used directly. All other concentrations are derived from online injection peak areas and the power law calibration shown in Fig. S2a.

[ˇ]uncertainty on methoxyl concentration, estimated from error envelope on linear calibrations shown in Figs. S2b,c.

[ˆ]1 standard error (1 s.e. = $1\sigma/\sqrt{n}$) uncertainty of methoxyl $\delta^{13}C$ values of replicate injections. For samples where n = 1, we adopt the long-term 1σ of injections of the CH_3I standard (1.6 ‰, n = 18).

[+]Vitrinite reflectance, compiled from literature sources (see Materials and Methods Section 1 for details).

[“]Bulk elemental contents of USC Bamboo and Poplar wood not determined, but rather derived from literature sources: ref. (*70*) for bamboo, and ref. (*71*) for poplar.

[*]Methoxyl carbon fraction = (Wt.% methoxyl/31.034)×(12.011/Wt.% C)×(1/lignin fraction). Lignin fraction is the fraction of all carbon atoms that are in lignin or lignin-derived products. Here we assume lignin fractions are 0.25 for wood, and 1.0 for all other samples. This accounts for the observation that during early diagenesis other wood components (cellulose, hemicellulose, extractives) are quantitatively removed while leaving the lignin structure essentially intact (*5*). See Materials and Methods section 4. for further details.

Table S2.

Methoxyl-derived iodomethane concentration and $\delta^{13}C$ values from individual headspace injections of samples derivatized and measured by online GC-combustion-IRMS.

Type	Name	Date	Reaction amount (mg)	Injection size (µL)	Rel. time (s)	CH_3I area (Vs)	CH_3I $\delta^{13}C$ (‰ vs. VPDB)	Area normalized (Vs/µL/mg)
Wood	USC Bamboo	10/18/17	2.4	250	130.8	13.832	-28.38	0.023053
Wood	USC Poplar	10/19/17	9.2	50	130.4	9.506	-27.90	0.020665
Wood	USC Poplar	10/20/17	9.2	250	131.6	47.145	-28.02	0.020498
Wood	USC Poplar	10/28/17	9.2	250	131.6	46.072	-27.94	0.020031
Wood	USC Poplar	10/19/17	9.8	250	132	59.459	-27.94	0.024269
Lignin std	USC Lignin	10/19/17	5.9	50	131.2	11.29	-21.29	0.038271
Lignin std	USC Lignin	10/19/17	5.9	250	132.1	64.33	-21.32	0.043614
Belchatow lignite	PL-4/384	10/23/17	146.7	10	131.8	48.876	-18.93	0.033317
Belchatow lignite	PL-4/384	10/23/17	146.7	10	131.9	40.837	-19.02	0.027837
Belchatow lignite	PL-11/384	10/23/17	105.9	10	130.1	27.698	-13.17	0.026155
Belchatow lignite	PL-11/384	10/23/17	105.9	10	131.4	29.074	-13.15	0.027454
Shimokita coal	IODP-337 15R3	10/29/17	856.9	250	130.9	9.735	13.64	4.54E-05
Shimokita coal	IODP-337 15R4	10/28/17	195.8	250	131.1	8.446	6.50	0.000173
Shimokita coal	IODP-337 15R7	10/21/17	1168	250	131.1	6.176	9.81	2.12E-05
Shimokita coal	IODP-337 15R7	10/22/17	1168	250	130.8	4.511	13.84	1.54E-05
Shimokita coal	IODP-337 15R7	10/22/17	1168	250	130.5	3.579	14.48	1.23E-05
Shimokita coal	IODP-337 18R2	10/20/17	343	250	130.7	30.545	22.13	0.000356
Shimokita coal	IODP-337 18R2	10/20/17	343	25	131.2	2.397	22.79	0.00028
Shimokita coal	IODP-337 18R2	10/20/17	343	250	129.9	19.912	22.60	0.000232
Shimokita coal	IODP-337 22R5	11/2/17	564.1	250	131.6	6.701	27.87	4.75E-05
Shimokita coal	IODP-337 22R5	11/1/17	564.1	250	131.2	8.71	26.82	6.18E-05
Shimokita coal	IODP-337 22R5	11/1/17	564.1	25	130.2	1.113	27.31	7.89E-05
Shimokita coal	IODP-337 25R	10/28/17	402.5	250	130.2	81.867	18.14	0.000814
Shimokita coal	IODP-337 25R	10/28/17	402.5	50	131.3	15.155	18.10	0.000753
Powder River coal	PR-FU S352	10/23/17	1132	250	132.5	3.441	12.73	1.22E-05
Powder River coal	PR-FU S939	10/29/17	1151.6	250	131.5	1.877	4.55	6.52E-06

Table S3

Methoxyl-derived iodomethane abundances and $\delta^{13}C$ values from offline derivatization, purification, and sealed-tube combustion + IRMS procedure

Type	Name	Reaction date	Reaction amount (mg)	CH_3I abundance (μmol)	CH_3I $\delta^{13}C$ (‰ vs. VPDB)	Wt.% methoxyl
Wood	USC Bamboo	1/31/16	63	84.80	-30.36	4.18E+00
Wood	USC Poplar	12/16/16	125.8	184.43	-27.77	4.55E+00
Belchatow lignite	PL-4/384	10/12/16	110	340.85	-20.50	9.62E+00
Belchatow lignite	PL-11/384	10/11/16	527.1	1135.86	-13.59	6.69E+00
Shimokita coal	IODP-337 15R3	6/12/16	2500	119.83	20.57	1.49E-01
Shimokita coal	IODP-337 15R4	10/6/16	2592	118.36	6.73	1.42E-01
Shimokita coal	IODP-337 15R7	10/5/16	2349	96.68	-13.98	1.28E-01
Shimokita coal	IODP-337 18R2	4/12/16	11400	246.86	23.46	6.72E-02
Shimokita coal	IODP-337 18R2	6/12/16	5500	151.68	29.69	8.56E-02
Shimokita coal	IODP-337 18R2	9/29/16	2745	192.64	22.49	2.18E-01
Shimokita coal	IODP-337 22R5	10/2/16	3275	66.30	16.69	6.28E-02
Powder River coal	PR-FU S352	7/23/17	7240	101.42	-2.02	4.35E-02
Powder River coal	PR-FU S939	7/24/17	9380	121.98	-21.45	4.04E-02
DM*	DM-P-1	7/1/17	65.8	142.08	-21.67	6.70E+00
DM*	DM-P-2	7/1/17	93.5	206.46	-14.67	6.85E+00

*DM: Demethylation reaction. Measurement of methoxyl groups from pyrolysis experiments. See Table S4 for details.

Table S4

Conditions and results of dry, open system pyrolysis experiments using USC Poplar wood.

Name	Pyrolysis date	Pyrolysis T (°C)	Pyrolysis time (hrs)	Initial mass (mg)	Final mass (mg)	Wt.% methoxyl[†]	F*
USC Poplar	12/16/16	N/A	N/A	125.0	125.0	4.55	1.00
DM-P-1	7/1/17	300	12.5	298.1	118.6	6.70	0.59
DM-P-2	7/2/17	300	34.0	416.0	93.7	6.85	0.34

[†]Wt.% methoxyl computed from offline reactions listed in Table S3.

*Fraction of methoxyl groups remaining. Computed by comparing the moles of methoxyl groups remaining (from the mass remaining and the methoxyl concentration determined in Table S3) to the expected initial moles of methoxyl groups (from the initial mass and the methoxyl concentration of unreacted poplar wood).

Table S5

Compilation of measured and theoretical carbon isotope effects for the degradation of methoxyl groups in a variety of scenarios.

Mechanism	Range of $^{13}\varepsilon$ (‰)	Source	Description of source and comments on use here
Homolytic C–O cleavage (40–75°C)	–45.8 to –55.1‰	Tang et al., 2000 (*17*)	Transition-state model with Arrhenian temperature dependence, computed at 100–500K. We compared epsilons for methanol and di-methyl ether, which agreed within 1‰ at all T of interest. So, we took the larger range.
S_N1 reaction	~0 to –30 ‰	Elsner et al., 2005 (*72*)	Conservative estimate for the range of kinetic isotope effects expected during degradation of MTBE (or a methoxyl group, generally) by an S_N1 mechanism. This agrees with experimental data for acid hydrolysis (see succeeding rows).
Methyl group oxidation	–10 to –30 ‰	Elsner et al., 2005 (*72*)	Conservative estimate for the range of kinetic isotope effects expected during oxidation of the methoxyl group in MTBE (or, generally).
S_N2 reaction	–30 to –83 ‰	Elsner et al., 2005 (*72*)	Conservative estimate for the range of kinetic isotope effects expected during degradation of MTBE (or a methoxyl group, generally) by an S_N2 mechanism. This agrees with culture data for anaerobic methylotrophy (see below).
Acid hydrolysis	–24.3 ± 2.3 ‰	Elsner et al., 2007 (*47*)	1200 ppm of MTBE was hydrolyzed at room-temperature in 2M HCl. Only the $^{13}\varepsilon$ for the entire residual MTBE molecule was measured (–4.9±0.6‰). This site-specific $^{13}\varepsilon$ assumes this observed fractionation is due entirely to an isotope effect at the reactive position (the methoxyl group, i.e., no secondary isotope effects). Elsner et al. speculate that some secondary isotope effects probably exist because this $^{13}\varepsilon$ is at the upper end of what would be expected for an SN1-type reaction such as this. This was confirmed by Julien et al. (2020), below. Nonetheless, we use this more negative value because it results in the widest range of possible values and most conservative estimates.
Acid hydrolysis	–16.8 ± 1.0‰	Julien et al., 2020 (*73*)	0.3 mM of MTBE was hydrolyzed at room-temperature in 250 mM of aqueous sulfuric acid. The isotope effect at the methoxyl group was calculated as the difference between the whole-molecule isotope effect (measured by GC-combustion-IRMS) and the isotope effect on the other methyl groups (measured by irm-^{13}C NMR). This is the only study to determine the site-specific isotope effect of acid hydrolysis without assumptions. However, the agreement between the bulk isotope effect in this work and those of previous studies suggests that it is representative of this reaction.
Permanganate oxidation	–24.3 ± 0.5‰	Gauchotte et al., 2010 (*74*)	2800 ppm of MTBE was oxidized at room-temperature in 0.5M $KMnO_4$. The isotope effect at the methoxyl group was determined by on-line GC-pyrolysis-GC-combustion-IRMS. Gauchotte do not determine the position-specific isotope effect at the methoxyl group directly, but because they observe no enrichment at the other methyl groups, it suggests minimal secondary isotope effects.
Permanganate oxidation	–16.8 ± 1.0 ‰	Julien et al., 2020 (*73*)	0.3 mM of MTBE was oxidized at room-temperature in 0.1M $KMnO_4$. The isotope effect at the methoxyl group was calculated as the difference between the whole-molecule isotope effect (measured by GC-combustion-IRMS) and the isotope effect on the other methyl groups (measured by irm-^{13}C NMR).
Aerobic biodegradation	–11.5 ± 1.0 ‰*	Mckelvie et al., 2009 (*48*)	1000 ppm of MTBE was biodegraded at room-temperature by *Pseudocarnia* K1 in a pure laboratory culture.
Aerobic biodegradation	–11.0 ± 0.5 ‰ *	Gray et al., 2002 (*75*)	MTBE was biodegraded at room-temperature by a pure culture of *M. Petroleiphilum* PM1.
Aerobic biodegradation	–7.5 to 9.0 ‰ *	Gray et al., 2002 (*75*)	MTBE was biodegraded in a sediment + groundwater microcosm with a mixed consortia sampled from Vandenburg AFB.
Aerobic biodegradation	–2.5 ± 0.5 ‰ *	Rosell et al., 2007 (*76*)	100–200 ppm MTBE was biodegraded at 30°C by a pure culture of *β*-protebacterium L108, isolated from MTBE-contaminated groundwater in Luena, Germany.
Aerobic biodegradation	–12.0 ± 0.5 ‰ *	Rosell et al., 2007 (*76*)	100–200 ppm MTBE was biodegraded at 30 °C by a pure culture of *Methylibium* R8.
Aerobic biodegradation	–0.9 ± 0.5 ‰ *	Rosell et al., 2007 (*76*)	100–200 ppm MTBE was biodegraded at 30 °C by a pure culture of *Rhodococcus ruber* IFP2001.
Aerobic biodegradation	–7.6 to –9.9 ‰ *	Hunkeler et al., 2001(*77*)	10 ppm MTBE was biodegraded at room temperature in a sand + groundwater microcosm containing a microbial consortium enriched from the Borden aquifer near Alliston, ON.
Aerobic Biodegradation	As large as –15‰	Anhauser et al., 2015 (*78*)	Environmental methoxyl degradation experiments where the methoxyl concentration and isotope compositions of senescent leaf litter was monitored over the course of ~3 yrs. –15‰ is the maximum isotope effect seen in this data. Note that because only whole-leaf methoxyl compositions were measured, these isotope enrichments may alternatively be due to the preferential loss of compounds more labile than lignin with lower methoxyl 13C contents (e.g., pectin, chlorophyll). See Fig. S11 for details.
Anaerobic biodegradation	–46 ± 25 ‰ *	Kolhatkar et al., 2002 (*79*)	0.7–6.0 ppm MTBE was biodegraded anaerobically at room temperature in sand + groundwater microcosms containing a microbial consortium sampled from a

			polluted well at a retail gasoline station in New Jersey.
Anaerobic biodegradation	–41 ± 4 ‰ *	Kolhatkar et al., 2002 (*79*)	Field study of water samples from a polluted well at a retail gasoline station in New Jersey.
Anaerobic biodegradation	–50 to –70 ‰ *	Kuder et al., 2005 (*80*)	100 ppm MTBE was biodegraded anaerobically at room temperature in cultures enriched from the microcosm experiments described in Kolhatkar et al., 2002
Anaerobic biodegradation	–78 ± 21 ‰ *	Somsamak et al., 2005 (*81*)	20 ppm MTBE was biodegraded anaerobically at 28°C in cultures enriched from a methanogenic sediment inoculum from Arthur Kill inlet, between NJ and Staten Island, NY
Anaerobic biodegradation	–72 ± 3.5 ‰ *	Somsamak et al., 2006 (*82*)	20 ppm MTBE was biodegraded anaerobically at 28°C in either methanogenic or sulfate reducing conditions with cultures enriched from methanogenic sediment inoculum from Coronado Cays, CA or Arthur Kill inlet, above.
Anaerobic biodegradation	–72 to –77 ‰	Oremland et al. 1982 (*83*)	Enrichment culture of methanogenic sediment slurries from Big Soda Lake, NV, grown on methanol. Although not known at the time, later work has established that the initial step of methylotrophic methanogenesis involves cleaving the methanol C–O bond and tranfer of the methyl group to methyl-S-CoM by methylcobalamin:coenzyme M methyltransferase (e.g., Londry et al., (*18*))
Anaerobic biodegradation	–72 to –83 ‰	Penger et al., 2012 (*84*)	Pure cultures of the methanogens *Methanosarcina barkeri*, *Methanosarcina acetivorans*, and *Methanolobus zinderi* were grown on methanol at 37°C. These isotope effects are specifically for methanol consumption under these substrate-replete conditions
Anaerobic biodegradation	–57 ‰	Freude & Blaser, 2016 (*85*)	Pure cultures of the acetogenic bacteria *Sporomusa sphaeroides* were grown on methanol at 30°C. These isotope effects are specifically for methanol consumption under these substrate-replete conditions

* Isotope effect at the methoxyl group of MTBE is estimated as 5 $\times^{13}\varepsilon$ of the whole molecule, which assumes no secondary isotope effects. See Elsner et al., 2007 for details.

Table S6

Compilation of $\delta^{13}C_{methoxyl}$ and methoxyl concentration (where available) from previous studies.

Sample ID	$\delta^{13}C_{methoxyl}$ (‰ vs. VPDB)	wt.% methoxyl	Source
USC poplar	-26.8	4.55	Lee et al., 2019 (*32*)
HUBG3	-29.4	4.71	Greule et al., 2019 (*56*)
HUBG4	-30.17	5.4	Greule et al., 2019
HUBG5	-29.6	5.09	Greule et al., 2019
USGS54	-25.63	3.97	Greule et al., 2019
USGS55	-32.66	3.98	Greule et al., 2019
USGS56	-27.97	4.2	Greule et al., 2019
European ash (Fraxinus excelsior)	-24.8		Greule et al., 2009 (*55*)
English oak (Quercus robur)	-28		Greule et al., 2009
Sweet osmanthus (Osmanthus fragans)	-27.3		Greule et al., 2009
Geronggang (Cratoxylum sp.)	-25		Greule et al., 2009
Dark red maranti (Shorea sp.)	-25.4		Greule et al., 2009
Utile (Entandrophragma utile)	-26.5		Greule et al., 2009
Pinus sylvestris (min. value)	-23.2		Mischel et al., 2016 (*86*)
Pinus sylvestris (max. value)	-21.6		Mischel et al., 2016
Larix decidua; Tree 1 (min. value)	-29		Riechelmann et al., 2016 (*87*)
Larix decidua; Tree 1 (max. value)	-23.5		Riechelmann et al., 2016
Larix decidua; Tree 2 (min. value)	-28.2		Riechelmann et al., 2016
Larix decidua; Tree 2 (max. value)	-22		Riechelmann et al., 2016
Larix decidua; Tree 3 (min. value)	-26		Riechelmann et al., 2016
Larix decidua; Tree 3 (max. value)	-22.2		Riechelmann et al., 2016
Larix decidua; Tree 4 (min. value)	-27		Riechelmann et al., 2016
Larix decidua; Tree 4 (max. value)	-24		Riechelmann et al., 2016
Larix decidua; Tree 5 (min. value)	-27.5		Riechelmann et al., 2016
Larix decidua; Tree 5 (max. value)	-24		Riechelmann et al., 2016
Picea abies, Cermis (min. value)	-22		Gori et al., 2012 (*58*)
Picea abies, Cermis (max. value)	-20		Gori et al., 2012
Picea abies, Val Maggiore (min. value)	-21		Gori et al., 2012
Picea abies, Val Maggiore (max. value)	-20		Gori et al., 2012
Picea abies, Baselga (min. value)	-23.5		Gori et al., 2012
Picea abies, Baselga (max. value)	-19		Gori et al., 2012

References and Notes

1. World Energy Resources 2016 (World Energy Council, 2016); www.worldenergy.org/publications/entry/world-energy-resources-2016.

2. D. Ritter, D. Vinson, E. Barnhart, D. M. Akob, M. W. Fields, A. B. Cunningham, W. Orem, J. C. McIntosh, Enhanced microbial coalbed methane generation: A review of research, commercial activity, and remaining challenges. *Int. J. Coal Geol.* **146**, 28–41 (2015). doi:10.1016/j.coal.2015.04.013

3. M. Saunois, A. R. Stavert, B. Poulter, P. Bousquet, J. G. Canadell, R. B. Jackson, P. A. Raymond, E. J. Dlugokencky, S. Houweling, P. K. Patra, P. Ciais, V. K. Arora, D. Bastviken, P. Bergamaschi, D. R. Blake, G. Brailsford, L. Bruhwiler, K. M. Carlson, M. Carrol, S. Castaldi, N. Chandra, C. Crevoisier, P. M. Crill, K. Covey, C. L. Curry, G. Etiope, C. Frankenberg, N. Gedney, M. I. Hegglin, L. Höglund-Isaksson, G. Hugelius, M. Ishizawa, A. Ito, G. Janssens-Maenhout, K. M. Jensen, F. Joos, T. Kleinen, P. B. Krummel, R. L. Langenfelds, G. G. Laruelle, L. Liu, T. Machida, S. Maksyutov, K. C. McDonald, J. McNorton, P. A. Miller, J. R. Melton, I. Morino, J. Müller, F. Murguia-Flores, V. Naik, Y. Niwa, S. Noce, S. O'Doherty, R. J. Parker, C. Peng, S. Peng, G. P. Peters, C. Prigent, R. Prinn, M. Ramonet, P. Regnier, W. J. Riley, J. A. Rosentreter, A. Segers, I. J. Simpson, H. Shi, S. J. Smith, L. P. Steele, B. F. Thornton, H. Tian, Y. Tohjima, F. N. Tubiello, A. Tsuruta, N. Viovy, A. Voulgarakis, T. S. Weber, M. van Weele, G. R. van der Werf, R. F. Weiss, D. Worthy, D. Wunch, Y. Yin, Y. Yoshida, W. Zhang, Z. Zhang, Y. Zhao, B. Zheng, Q. Zhu, Q. Zhu, Q. Zhuang, The Global Methane Budget 2000–2017. *Earth Syst. Sci. Data* **12**, 1561–1623 (2020). doi:10.5194/essd-12-1561-2020

4. A. J. Turner, C. Frankenberg, E. A. Kort, Interpreting contemporary trends in atmospheric methane. *Proc. Natl. Acad. Sci. U.S.A.* **116**, 2805–2813 (2019). doi:10.1073/pnas.1814297116 Medline

5. D. Rice, Composition and origins of coalbed gas. *AAPG Stud. Geol.* **38**, 159–184 (1993).

6. D. Strąpoć, M. Mastalerz, K. Dawson, J. Macalady, A. V. Callaghan, B. Wawrik, C. Turich, M. Ashby, Biogeochemistry of Microbial Coal-Bed Methane. *Annu. Rev. Earth Planet. Sci.* **39**, 617–656 (2011). doi:10.1146/annurev-earth-040610-133343

7. P. G. Hatcher, D. J. Clifford, The organic geochemistry of coal: From plant materials to coal. *Org. Geochem.* **27**, 251–274 (1997). doi:10.1016/S0146-6380(97)00051-X

8. C. Durand-Souron, R. Boulet, B. Durand, Formation of methane and hydrocarbons by pyrolysis of immature kerogens. *Geochim. Cosmochim. Acta* **46**, 1193–1202 (1982). doi:10.1016/0016-7037(82)90005-9

9. I. Blom, L. Edelhausen, D. W. van Krevelen, Chemical structure and properties of Coal XVIII–Oxygen groups in coal and related products. *Fuel* **36**, 135–153 (1957).

10. D. F. Payne, P. J. Ortoleva, A model for lignin alteration—part I: A kinetic reaction-network model. *Org. Geochem.* **32**, 1073–1085 (2001). doi:10.1016/S0146-6380(01)00080-8

11. J. Heider, G. Fuchs, Anaerobic metabolism of aromatic compounds. *Eur. J. Biochem.* **243**, 577–596 (1997). doi:10.1111/j.1432-1033.1997.00577.x Medline

12. D. Mayumi, H. Mochimaru, H. Tamaki, K. Yamamoto, H. Yoshioka, Y. Suzuki, Y. Kamagata, S. Sakata, Methane production from coal by a single methanogen. *Science* **354**, 222–225 (2016). doi:10.1126/science.aaf8821 Medline

13. F. Inagaki, K. U. Hinrichs, Y. Kubo, M. W. Bowles, V. B. Heuer, W. L. Hong, T. Hoshino, A. Ijiri, H. Imachi, M. Ito, M. Kaneko, M. A. Lever, Y. S. Lin, B. A. Methé, S. Morita, Y. Morono, W. Tanikawa, M. Bihan, S. A. Bowden, M. Elvert, C. Glombitza, D. Gross, G. J. Harrington, T. Hori, K. Li, D. Limmer, C. H. Liu, M. Murayama, N. Ohkouchi, S. Ono, Y. S. Park, S. C. Phillips, X. Prieto-Mollar, M. Purkey, N. Riedinger, Y. Sanada, J. Sauvage, G. Snyder, R. Susilawati, Y. Takano, E. Tasumi, T. Terada, H. Tomaru, E. Trembath-Reichert, D. T. Wang, Y. Yamada, Exploring deep microbial life in coal-bearing sediment down to ~2.5 km below the ocean floor. *Science* **349**, 420–424 (2015). doi:10.1126/science.aaa6882 Medline

14. V. B. Heuer, F. Inagaki, Y. Morono, Y. Kubo, A. J. Spivack, B. Viehweger, T. Treude, F. Beulig, F. Schubotz, S. Tonai, S. A. Bowden, M. Cramm, S. Henkel, T. Hirose, K. Homola, T. Hoshino, A. Ijiri, H. Imachi, N. Kamiya, M. Kaneko, L. Lagostina, H. Manners, H.-L. McClelland, K. Metcalfe, N. Okutsu, D. Pan, M. J. Raudsepp, J. Sauvage, M.-Y. Tsang, D. T. Wang, E. Whitaker, Y. Yamamoto, K. Yang, L. Maeda, R. R. Adhikari, C. Glombitza, Y. Hamada, J. Kallmeyer, J. Wendt, L. Wörmer, Y. Yamada, M. Kinoshita, K.-U. Hinrichs, Temperature limits to deep subseafloor life in the Nankai Trough subduction zone. *Science* **370**, 1230–1234 (2020). doi:10.1126/science.abd7934 Medline

15. M. J. Whiticar, Carbon and hydrogen isotope systematics of bacterial formation and oxidation of methane. *Chem. Geol.* **161**, 291–314 (1999). doi:10.1016/S0009-2541(99)00092-3

16. C. Clayton, Carbon isotope fractionation during natural gas generation from kerogen. *Mar. Pet. Geol.* **8**, 232–240 (1991). doi:10.1016/0264-8172(91)90010-X

17. Y. Tang, J. K. Perry, P. D. Jenden, M. Schoell, Mathematical modeling of stable carbon isotope ratios in natural gases. *Geochim. Cosmochim. Acta* **64**, 2673–2687 (2000). doi:10.1016/S0016-7037(00)00377-X

18. K. L. Londry, K. G. Dawson, H. D. Grover, R. E. Summons, A. S. Bradley, Stable carbon isotope fractionation between substrates and products of *Methanosarcina barkeri*. *Org. Geochem.* **39**, 608–621 (2008). doi:10.1016/j.orggeochem.2008.03.002

19. J. B. Best, The inference of intracellular enzymatic properties from kinetic data obtained on living cells. I. Some kinetic considerations regarding an enzyme enclosed by a diffusion barrier. *J. Cell. Comp. Physiol.* **46**, 1–27 (1955). doi:10.1002/jcp.1030460102 Medline

20. T. N. P. Bosma, P. J. M. Middeldorp, G. Schraa, A. J. B. Zehnder, Mass Transfer Limitation of Biotransformation: Quantifying Bioavailability. *Environ. Sci. Technol.* **31**, 248–252 (1996). doi:10.1021/es960383u

21. M. Thullner, M. Kampara, H. H. Richnow, H. Harms, L. Y. Wick, Impact of bioavailability restrictions on microbially induced stable isotope fractionation. 1. Theoretical calculation. *Environ. Sci. Technol.* **42**, 6544–6551 (2008). doi:10.1021/es702782c Medline

22. S. J. B. Mallinson, M. M. Machovina, R. L. Silveira, M. Garcia-Borràs, N. Gallup, C. W. Johnson, M. D. Allen, M. S. Skaf, M. F. Crowley, E. L. Neidle, K. N. Houk, G. T. Beckham, J. L. DuBois, J. E. McGeehan, A promiscuous cytochrome P450 aromatic *O*-demethylase for lignin bioconversion. *Nat. Commun.* **9**, 2487 (2018). doi:10.1038/s41467-018-04878-2 Medline

23. D. Naidu, S. W. Ragsdale, Characterization of a three-component vanillate *O*-demethylase from *Moorella thermoacetica*. *J. Bacteriol.* **183**, 3276–3281 (2001). doi:10.1128/JB.183.11.3276-3281.2001 Medline

24. L. Gao, M. Mastalerz, A. Schimmelmann, in *Coal Bed Methane: From Prospect to Pipeline*, P. Thakur, S. Schatzel, K. Aminian, Eds. (Elsevier, 2014), pp. 7–29.

25. F. Keppler, R. M. Kalin, D. B. Harper, W. C. Mcroberts, J. T. G. Hamilton, Carbon isotope anomaly in the major plant C_1 pool and its global biogeochemical implications. *Biogeosciences* **1**, 123–131 (2004). doi:10.5194/bg-1-123-2004

26. E. Trembath-Reichert, Y. Morono, A. Ijiri, T. Hoshino, K. S. Dawson, F. Inagaki, V. J. Orphan, Methyl-compound use and slow growth characterize microbial life in 2-km-deep subseafloor coal and shale beds. *Proc. Natl. Acad. Sci. U.S.A.* **114**, E9206–E9215 (2017). doi:10.1073/pnas.1707525114 Medline

27. S. A. Bowden, A. Y. Mohamed, A. N. F. Edilbi, Y.-S. Lin, Y. Morono, K.-U. Hinrichs, F. Inagaki, Modelling the Shimokita deep coalbed biosphere over deep geological time: Starvation, stimulation, material balance and population models. *Basin Res.* **32**, 804–829 (2020). doi:10.1111/bre.12399

28. B. Wawrik, M. Mendivelso, V. A. Parisi, J. M. Suflita, I. A. Davidova, C. R. Marks, J. D. Van Nostrand, Y. Liang, J. Zhou, B. J. Huizinga, D. Strąpoć, A. V. Callaghan, Field and laboratory studies on the bioconversion of coal to methane in the San Juan Basin. *FEMS Microbiol. Ecol.* **81**, 26–42 (2012). doi:10.1111/j.1574-6941.2011.01272.x Medline

29. M. Schoell, Genetic Characterization of Natural Gases. *AAPG Bull.* **67**, 2225–2238 (1983).

30. M. J. Whiticar, Stable isotope geochemistry of coals, humic kerogens and related natural gases. *Int. J. Coal Geol.* **32**, 191–215 (1996). doi:10.1016/S0166-5162(96)00042-0

31. D. S. Vinson, N. E. Blair, A. M. Martini, S. Larter, W. H. Orem, J. C. McIntosh, Microbial methane from in situ biodegradation of coal and shale: A review and reevaluation of hydrogen and carbon isotope signatures. *Chem. Geol.* **453**, 128–145 (2017). doi:10.1016/j.chemgeo.2017.01.027

32. H. Lee, X. Feng, M. Mastalerz, S. J. Feakins, Characterizing lignin: Combining lignin phenol, methoxy quantification, and dual stable carbon and hydrogen isotopic techniques. *Org. Geochem.* **136**, 103894 (2019). doi:10.1016/j.orggeochem.2019.07.003

33. O. A. Sherwood, S. Schwietzke, V. A. Arling, G. Etiope, Global Inventory of Gas Geochemistry Data from Fossil Fuel, Microbial and Burning Sources, version 2017. *Earth Syst. Sci. Data* **9**, 639–656 (2017). doi:10.5194/essd-9-639-2017

34. A. Drobniak, M. Mastalerz, Chemical evolution of Miocene wood: Example from the Belchatow brown coal deposit, central Poland. *Int. J. Coal Geol.* **66**, 157–178 (2006). doi:10.1016/j.coal.2005.06.004

35. F. Inagaki, K.-U. Hinrichs, Y. Kubo, IODP Expedition 337 Scientists, IODP Expedition 337: Deep Coalbed Biosphere off Shimokita – Microbial processes and hydrocarbon system associated with deeply buried coalbed in the ocean. *Sci. Drill.* **21**, 17–28 (2016). doi:10.5194/sd-21-17-2016

36. D. Gross, A. Bechtel, G. J. Harrington, Variability in coal facies as reflected by organic petrological and geochemical data in Cenozoic coal beds offshore Shimokita (Japan) - IODP Exp. 337. *Int. J. Coal Geol.* **152**, 63–79 (2015). doi:10.1016/j.coal.2015.10.007

37. F. Inagaki, K.-U. Hinrichs, Y. Kubo, Expedition 337 Scientists, "Deep Coalbed Biosphere off Shimokita" in *Proceedings of the Integrated Ocean Drilling Program* (Integrated Ocean Drilling Program, 2013); http://publications.iodp.org/proceedings/337/337title.htm.

38. M. Formolo, A. Martini, S. Petsch, Biodegradation of sedimentary organic matter associated with coalbed methane in the Powder River and San Juan Basins, USA. *Int. J. Coal Geol.* **76**, 86–97 (2008). doi:10.1016/j.coal.2008.03.005

39. R. M. Flores, C. A. Rice, G. D. Stricker, A. Warden, M. S. Ellis, Methanogenic pathways of coal-bed gas in the Powder River Basin, United States: The geologic factor. *Int. J. Coal Geol.* **76**, 52–75 (2008). doi:10.1016/j.coal.2008.02.005

40. R. M. Flores, "Styles of coal deposition in Tertiary alluvial deposits, Powder River Basin, Montana and Wyoming" in *Paleoenvironmental and Tectonic Controls in Coal-Forming Basins in the United States*, P. C. Lyons, C. L. Rice, (Geological Society of America, 1986).

41. P. G. Hatcher, H. E. Lerch III, R. K. Kotra, T. V. Verheyen, Pyrolysis, g.c.—m.s. of a series of degraded woods and coalified logs that increase in rank from peat to subbituminous coal. *Fuel* **67**, 1069–1075 (1988). doi:10.1016/0016-2361(88)90372-9

42. P. G. Hatcher, I. A. Breger, N. Szeverenyi, G. E. Maciel, Nuclear magnetic resonance studies of ancient buried wood—II. Observations on the origin of coal from lignite to bituminous coal. *Org. Geochem.* **4**, 9–18 (1982). doi:10.1016/0146-6380(82)90003-1

43. M. A. Rooney, G. E. Claypool, H. M. Chung, Modeling thermogenic gas generation using carbon isotope ratios of natural gas hydrocarbons. *Chem. Geol.* **126**, 219–232 (1995). doi:10.1016/0009-2541(95)00119-0

44. B. Cramer, E. Faber, P. Gerling, B. M. Krooss, Reaction Kinetics of Stable Carbon Isotopes in Natural GasInsights from Dry, Open System Pyrolysis Experiments. *Energy Fuels* **15**, 517–532 (2001). doi:10.1021/ef000086h

45. J. T. G. Hamilton, W. C. McRoberts, F. Keppler, R. M. Kalin, D. B. Harper, Chloride methylation by plant pectin: An efficient environmentally significant process. *Science* **301**, 206–209 (2003). doi:10.1126/science.1085036 Medline

46. F. Keppler, J. T. G. Hamilton, W. C. McRoberts, I. Vigano, M. Braß, T. Röckmann, Methoxyl groups of plant pectin as a precursor of atmospheric methane: Evidence from deuterium labelling studies. *New Phytol.* **178**, 808–814 (2008). doi:10.1111/j.1469-8137.2008.02411.x Medline

47. M. Elsner, J. McKelvie, G. L. Couloume, B. S. Lollar, Insight into methyl *tert*-butyl ether (MTBE) stable isotope fractionation from abiotic reference experiments. *Environ. Sci. Technol.* **41**, 5693–5700 (2007). doi:10.1021/es070531o Medline

48. J. R. McKelvie, M. R. Hyman, M. Elsner, C. Smith, D. M. Aslett, G. Lacrampe-Couloume, B. S. Lollar, Isotopic fractionation of methyl *tert*-butyl ether suggests different initial reaction mechanisms during aerobic biodegradation. *Environ. Sci. Technol.* **43**, 2793–2799 (2009). doi:10.1021/es803307y Medline

49. F. Keppler, D. B. Harper, R. M. Kalin, W. Meier-Augenstein, N. Farmer, S. Davis, H.-L. Schmidt, D. M. Brown, J. T. G. Hamilton, Stable hydrogen isotope ratios of lignin methoxyl groups as a paleoclimate proxy and constraint of the geographical origin of wood. *New Phytol.* **176**, 600–609 (2007). doi:10.1111/j.1469-8137.2007.02213.x Medline

50. T. Anhäuser, M. Greule, D. Polag, G. J. Bowen, F. Keppler, Mean annual temperatures of mid-latitude regions derived from δ^2H values of wood lignin methoxyl groups and its implications for paleoclimate studies. *Sci. Total Environ.* **574**, 1276–1282 (2017). doi:10.1016/j.scitotenv.2016.07.189 Medline

51. T. Anhäuser, B. A. Hook, J. Halfar, M. Greule, F. Keppler, Earliest Eocene cold period and polar amplification - Insights from δ^2H values of lignin methoxyl groups of mummified wood. *Palaeogeogr. Palaeoclimatol. Palaeoecol.* **505**, 326–336 (2018). doi:10.1016/j.palaeo.2018.05.049

52. A. L. Sessions, S. P. Sylva, R. E. Summons, J. M. Hayes, Isotopic exchange of carbon-bound hydrogen over geologic timescales. *Geochim. Cosmochim. Acta* **68**, 1545–1559 (2004). doi:10.1016/j.gca.2003.06.004

53. A. Schimmelmann, A. L. Sessions, M. Mastalerz, Hydrogen isotopic (D/H) composition of organic matter during diagenesis and thermal maturation. *Annu. Rev. Earth Planet. Sci.* **34**, 501–533 (2006). doi:10.1146/annurev.earth.34.031405.125011

54. S. Zeisel, Über ein Verfahren zum quantitativen Nachweise von Methoxyl. *Monatsh. Chem.* **6**, 989–997 (1885). doi:10.1007/BF01554683

55. M. Greule, A. Mosandl, J. T. G. Hamilton, F. Keppler, A simple rapid method to precisely determine $^{13}C/^{12}C$ ratios of plant methoxyl groups. *Rapid Commun. Mass Spectrom.* **23**, 1710–1714 (2009). doi:10.1002/rcm.4057 Medline

56. M. Greule, H. Moossen, M. K. Lloyd, H. Geilmann, W. A. Brand, J. M. Eiler, H. Qi, F. Keppler, Three wood isotopic reference materials for δ^2H and $\delta^{13}C$ measurements of plant methoxy groups. *Chem. Geol.* **533**, 119428 (2020). doi:10.1016/j.chemgeo.2019.119428

57. S. H. Lamlom, R. A. Savidge, A reassessment of carbon content in wood: Variation within and between 41 North American species. *Biomass Bioenergy* **25**, 381–388 (2003). doi:10.1016/S0961-9534(03)00033-3

58. Y. Gori, R. Wehrens, M. Greule, F. Keppler, L. Ziller, N. La Porta, F. Camin, Carbon, hydrogen and oxygen stable isotope ratios of whole wood, cellulose and lignin methoxyl groups of *Picea abies* as climate proxies. *Rapid Commun. Mass Spectrom.* **27**, 265–275 (2013). doi:10.1002/rcm.6446 Medline

59. J. Levine, in *AAPG Studies in Geology: Hydrocarbons from Coal*, B. E. Law, D. D. Rice, Eds. (American Association of Petroleum Geologists, 1993), pp. 39–77.

60. R. C. Pettersen, in *The Chemistry of Solid Wood*, R. Rowell, Ed., vol. 207 of *Advances in Chemistry* (American Chemical Society, 1984), pp. 57–126.

61. S. D. Killops, V. J. Killops, *Introduction to Organic Geochemistry* (Wiley, 2013).

62. P. G. Hatcher, Dipolar-dephasing 13C NMR studies of decomposed wood and coalified xylem tissue: Evidence for chemical structural changes associated with defunctionalization of lignin structural units during coalification. *Energy Fuels* **2**, 48–58 (1988). doi:10.1021/ef00007a008

63. A. C. Frazer, L. Y. Young, A gram-negative anaerobic bacterium that utilizes o-methyl substituents of aromatic acids. *Appl. Environ. Microbiol.* **49**, 1345–1347 (1985). doi:10.1128/aem.49.5.1345-1347.1985 Medline

64. J. T. Gelwicks, J. B. Risatti, J. M. Hayes, Carbon isotope effects associated with aceticlastic methanogenesis. *Appl. Environ. Microbiol.* **60**, 467–472 (1994). doi:10.1128/aem.60.2.467-472.1994

65. A. C. Frazer, in *Acetogenesis*, H. L. Drake, Ed. (Springer, Chapman & Hall Microbiology Series, 1994), pp. 445–483.

66. L. G. Ljungdahl, The autotrophic pathway of acetate synthesis in acetogenic bacteria. *Annu. Rev. Microbiol.* **40**, 415–450 (1986). doi:10.1146/annurev.mi.40.100186.002215 Medline

67. L. Y. Young, A. C. Frazer, The fate of lignin and lignin-derived compounds in anaerobic environments. *Geomicrobiol. J.* **5**, 261–293 (1987). doi:10.1080/01490458709385973

68. J. M. Hayes, Fractionation of Carbon and Hydrogen Isotopes in Biosynthetic Processes. *Rev. Mineral. Geochem.* **43**, 225–277 (2001). doi:10.2138/gsrmg.43.1.225

69. Y. Tang, P. D. Jenden, A. Nigrini, S. C. Teerman, Modeling Early Methane Generation in Coal. *Energy Fuels* **10**, 659–671 (1996). doi:10.1021/ef950153l

70. W.-H. Chen, S.-H. Liu, T.-T. Juang, C.-M. Tsai, Y.-Q. Zhuang, Characterization of solid and liquid products from bamboo torrefaction. *Appl. Energy* **160**, 829–835 (2015). doi:10.1016/j.apenergy.2015.03.022

71. W. Kalkreuth, D. Brouillard, C. Roy, Optical and chemical characterization of solid residues obtained from vacuum pyrolysis of wood (aspen poplar). *Biomass* **10**, 27–45 (1986). doi:10.1016/0144-4565(86)90034-X

72. M. Elsner, L. Zwank, D. Hunkeler, R. P. Schwarzenbach, A new concept linking observable stable isotope fractionation to transformation pathways of organic pollutants. *Environ. Sci. Technol.* **39**, 6896–6916 (2005). doi:10.1021/es0504587 Medline

73. M. Julien, D. Gori, P. Höhener, R. J. Robins, G. S. Remaud, Intramolecular isotope effects during permanganate oxidation and acid hydrolysis of methyl *tert*-butyl ether. *Chemosphere* **248**, 125975 (2020). doi:10.1016/j.chemosphere.2020.125975 Medline

74. C. Gauchotte, G. Connal, G. O'Sullivan, R. M. Kalin, in *Environmental Forensics: Proceedings of the 2009 INEF Annual Conference*, R. D. Morrison, G. O'Sullivan, Eds. (Royal Society of Chemistry, 2010), pp. 60–70.

75. J. R. Gray, G. Lacrampe-Couloume, D. Gandhi, K. M. Scow, R. D. Wilson, D. M. Mackay, B. S. Lollar, Carbon and hydrogen isotopic fractionation during biodegradation of methyl *tert*-butyl ether. *Environ. Sci. Technol.* **36**, 1931–1938 (2002). doi:10.1021/es011135n Medline

76. M. Rosell, D. Barceló, T. Rohwerder, U. Breuer, M. Gehre, H. H. Richnow, Variations in $^{13}C/^{12}C$ and D/H enrichment factors of aerobic bacterial fuel oxygenate degradation. *Environ. Sci. Technol.* **41**, 2036–2043 (2007). doi:10.1021/es0616175 Medline

77. D. Hunkeler, B. J. Butler, R. Aravena, J. F. Barker, Monitoring biodegradation of methyl *tert*-butyl ether (MTBE) using compound-specific carbon isotope analysis. *Environ. Sci. Technol.* **35**, 676–681 (2001). doi:10.1021/es001338w Medline

78. T. Anhäuser, M. Greule, M. Zech, K. Kalbitz, C. McRoberts, F. Keppler, Stable hydrogen and carbon isotope ratios of methoxyl groups during plant litter degradation. *Isotopes Environ. Health Stud.* **51**, 143–154 (2015). doi:10.1080/10256016.2015.1013540 Medline

79. R. Kolhatkar, T. Kuder, P. Philp, J. Allen, J. T. Wilson, Use of compound-specific stable carbon isotope analyses to demonstrate anaerobic biodegradation of MTBE in groundwater at a gasoline release site. *Environ. Sci. Technol.* **36**, 5139–5146 (2002). doi:10.1021/es025704i Medline

80. T. Kuder, J. T. Wilson, P. Kaiser, R. Kolhatkar, P. Philp, J. Allen, Enrichment of stable carbon and hydrogen isotopes during anaerobic biodegradation of MTBE: Microcosm and field evidence. *Environ. Sci. Technol.* **39**, 213–220 (2005). doi:10.1021/es040420e Medline

81. P. Somsamak, H. H. Richnow, M. M. Häggblom, Carbon isotopic fractionation during anaerobic biotransformation of methyl *tert*-butyl ether and *tert*-amyl methyl ether. *Environ. Sci. Technol.* **39**, 103–109 (2005). doi:10.1021/es049368c Medline

82. P. Somsamak, H. H. Richnow, M. M. Häggblom, Carbon isotope fractionation during anaerobic degradation of methyl *tert*-butyl ether under sulfate-reducing and methanogenic conditions. *Appl. Environ. Microbiol.* **72**, 1157–1163 (2006). doi:10.1128/AEM.72.2.1157-1163.2006 Medline

83. R. S. Oremland, L. Marsh, D. J. Desmarais, Methanogenesis in big soda lake, nevada: An alkaline, moderately hypersaline desert lake. *Appl. Environ. Microbiol.* **43**, 462–468 (1982). doi:10.1128/aem.43.2.462-468.1982 Medline

84. J. Penger, R. Conrad, M. Blaser, Stable carbon isotope fractionation by methylotrophic methanogenic archaea. *Appl. Environ. Microbiol.* **78**, 7596–7602 (2012). doi:10.1128/AEM.01773-12

85. C. Freude, M. Blaser, Carbon Isotope Fractionation during Catabolism and Anabolism in Acetogenic Bacteria Growing on Different Substrates. *Appl. Environ. Microbiol.* **82**, 2728–2737 (2016). doi:10.1128/AEM.03502-15 Medline

86. M. Mischel, J. Esper, F. Keppler, M. Greule, W. Werner, $\delta^{2}H$, $\delta^{13}C$ and $\delta^{18}O$ from whole wood, α-cellulose and lignin methoxyl groups in *Pinus sylvestris*: A multi-parameter approach. *Isotopes Environ. Health Stud.* **51**, 553–568 (2016). doi:10.1080/10256016.2015.1056181 Medline

87. D. F. C. Riechelmann, M. Greule, K. Treydte, J. Esper, F. Keppler, Climate signals in $\delta^{13}C$ of wood lignin methoxyl groups from high-elevation larch trees. *Palaeogeogr. Palaeoclimatol. Palaeoecol.* **445**, 60–71 (2016). doi:10.1016/j.palaeo.2016.01.001

88. M. Greule, F. Keppler, Stable isotope determination of ester and ether methyl moieties in plant methoxyl groups. *Isotopes Environ. Health Stud.* **47**, 470–482 (2011). doi:10.1080/10256016.2011.616270 Medline